AD-A148 261 DEVELOPMENT OF A 20/30 GHZ RECEIVING STATION FOR PROPAGATION EXPERIMENTS W.. (U) UNIVERSIDAD POLITECNICA DE BARCELONA (SPAIN) ESCUELA TECNICA S.. A CARDAMA 1/1

UNCLASSIFIED 25 OCT 84 EOARD-TR-85-2 AFOSR-83-0337 F/G 20/14 NL

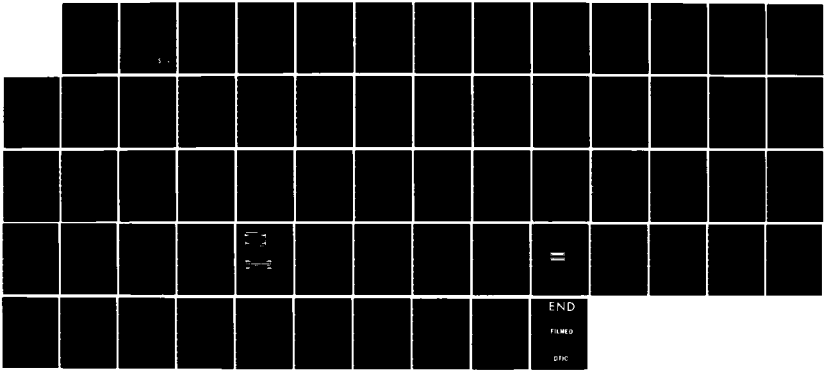

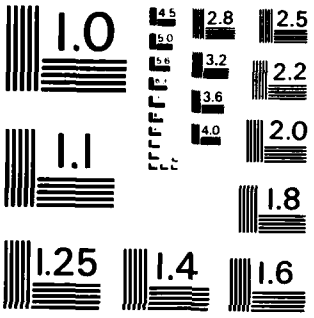

MICROCOPY RESOLUTION TEST CHART
NATIONAL BUREAU OF STANDARDS-1963-A

EOARD-TR-85 2

AD-A148 261

GRANT NO.: AFOSR-83-0337

DEVELOPMENT OF A 20/30 GHz RECEIVING STATION FOR PROPAGATION EXPERIMENTS WITH L-SAT

Angel Cardama
Universidad Politécnica de Barcelona
Escuela Técnica Superior
de Ingenieros de Telecomunicación
08034 - Barcelona - Spain

25 October 1984

Final Report, 1 September 1983 - 31 August 1984

Approved for public release;
distribution unlimited

Prepared for

EOARD/LNG
223/231 Old Marylebone Rd
London NW1 5TH, United Kingdom

DTIC FILE COPY

DTIC
ELECTE
DEC 5 1984
S D
A

84 12 03 033

SECURITY CLASSIFICATION OF THIS PAGE

REPORT DOCUMENTATION PAGE

1a. REPORT SECURITY CLASSIFICATION	1b. RESTRICTIVE MARKINGS
2a. SECURITY CLASSIFICATION AUTHORITY	3. DISTRIBUTION/AVAILABILITY OF REPORT
2b. DECLASSIFICATION/DOWNGRADING SCHEDULE	DISTRIBUTION UNLIMITED
4. PERFORMING ORGANIZATION REPORT NUMBER(S)	5. MONITORING ORGANIZATION REPORT NUMBER(S)
6a. NAME OF PERFORMING ORGANIZATION: UNIVERSIDAD POLITECNICA DE BARCELONA 6b. OFFICE SYMBOL (If applicable)	7a. NAME OF MONITORING ORGANIZATION
6c. ADDRESS (City, State and ZIP Code): ESCUELA TECNICA SUP. ING. TELECOMUNICACION APDO 30002 08034 - BARCELONA, SPAIN	7b. ADDRESS (City, State and ZIP Code)
8a. NAME OF FUNDING/SPONSORING ORGANIZATION: EOARD/LNG 8b. OFFICE SYMBOL (If applicable)	9. PROCUREMENT INSTRUMENT IDENTIFICATION NUMBER
8c. ADDRESS (City, State and ZIP Code): 223/231 OLD MARYLEBONE Rd LONDON NW1, 5TH, UK	10. SOURCE OF FUNDING NOS.

PROGRAM ELEMENT NO.	PROJECT NO.	TASK NO.	WORK UNIT NO.

11. TITLE (Include Security Classification): DEVELOPMENT OF A 20/30 GHZ RECEIVING STATION..

12. PERSONAL AUTHOR(S): ANGEL CARDAMA

13a. TYPE OF REPORT	13b. TIME COVERED	14. DATE OF REPORT (Yr., Mo., Day)	15. PAGE COUNT
FINAL REPORT	FROM 01-09-83 TO 31-08-84	1984-10-25	58

16. SUPPLEMENTARY NOTATION

17 COSATI CODES		
FIELD	GROUP	SUB GR

18. SUBJECT TERMS (Continue on reverse if necessary and identify by block number)

1 - PROPAGATION EXPERIMENT AT 20/30 GHz.
2 - 20/30 GHz SATELLITE RECEIVER.
3 - CYLINDRICAL NEAR FIELD RANGE.

19. ABSTRACT (Continue on reverse if necessary and identify by block number)

Basic technological work done on a 20/30 GHz L-SAT propagation experiment receiver is presented, covering receiver configuration, measurement systems, Gunn-diode oscillators, fin-line transitions and cylindrical near field antenna measurement systems.

20. DISTRIBUTION/AVAILABILITY OF ABSTRACT	21. ABSTRACT SECURITY CLASSIFICATION
UNCLASSIFIED/UNLIMITED ☐ SAME AS RPT. ☐ DTIC USERS ☐	

22a. NAME OF RESPONSIBLE INDIVIDUAL	22b. TELEPHONE NUMBER (Include Area Code)	22c. OFFICE SYMBOL
ANGEL CARDAMA	34-3-2046551	

DD FORM 1473, 83 APR EDITION OF 1 JAN 73 IS OBSOLETE

SECURITY CLASSIFICATION OF THIS PAGE

EOARD TR-85-02 10 November 1984

This report has been reviewed by the EOARD Information Office and is releasable to the National Technical Information Service (NTIS). At NTIS it will be releasable to the general public, including foreign nationals.

This technical report has been reviewed and is approved for publication.

JOHN D. WARBURTON
Major, USAF
Chief, Geophysics & Space

JACK D. MORRIS
Colonel, USAF
Commander

A1

P R E F A C E

This report covers the first of a three year research program intended to develop 20/30 GHz satellite receivers for the LSAT propagation experiment. The following staff members have participated in different parts of the research being reported:

Dr. Angel Cardama, Professor

Dr. Javier Bará, Professor

Dr. Elias de los Reyes, Associate Professor

Dr. Eduardo Artal, Associate Professor

Dr. Adolfo Comerón, Associate Porfessor

Dr. Ignacio Corbella, Associate Professor

Dr. Antonio Elias, Associate Professor

Dr. Miguel Ferrando, Associate Professor

Dr. Luis Jofre, Associate Professor

TABLE OF CONTENTS

1. INTRODUCTION

With the launching of LSAT, scheduled for early 1987, European research centers will have an unique opportunity to experiment for a minimum of five years on propagation and receiver engineering at 20/30 GHz.

In order to obtain attenuation and crosspolarization statistics in the city of Barcelona, where rainfall intensities of up to 450 millimeter hour have been recorded, a three year research program for in-house construction of a receiver has started with initial support from EOARD. In addition to the propagation experiment interest, the technonogical aspects of the receiver development, specially the 20/30 GHz front-ends, should be stressed.

This report covers basic technological work done in the program's first year, and includes five main research areas, presented in five corresponding sections.

The first section analyses the receiver configuration, establishing budget links and two possible receiver implementations of dissimilar complexity. It is followed by a presentation of the available measurement systems and the experimental set ups that are being planned. In the third section design data of K_a-band gunn-diode oscillators and their measurements are presented. The basic technologies employed in the construction of 20/30 GHz passive circuits are summarized in section four, also including design data of unilateral and antipodal fin-lines, that will be used in the construction of waveguide and microstrip transitions, and pin-diode modulators. The last section covers the work done in antenna measurement systems. A general formulation for field transformation from near-field measurements on a cylinder is presented, followed by an experimental study of the influence of the different range parameters and the definition of the 20/30 GHz cylindrical near-field range. Part of this work will be the subject of the paper "A Parametric Study of a Cylindrical Near-Field Antenna Measurement System" that will be presented at the International Symposium on Antennas, Nice, 13-15 November 1984.

2. LSAT BEACON RECEIVER

The future use of 20/30 GHz bands for Satellite Communications has prompted the European Space Agency (ESA) to include on board the L SAT satellite, now renamed OLYMPUS, a propagation package that will allow propagation experiments all over Europe at those frequencies.

The Olympus propagation package [1] includes three linearly polarized beacons, denoted B_0, B_1, B_2, operating at 12.502, 10.770 and 29.656 GHz respectively. All three frequencies are obtained from a high stability master oscillator by multiplication and are coherent. The 12.5 GHz beacon serves the study of frequency scaling of propagation characteristics and may be used as a tracking signal by earth station. The B_1 signal polarization will be switched at a rate of 933 Hz.

In principle there is a large set of possible measurements to be performed in the experiment: attenuation, crosspolarization discrimination, differential phase between copolar and crosspolar components, interchannel differential phase, scintillation, etc. our experimental plans are limited initially to attenuation measurements.

RECEIVER REQUIREMENTS

Each beacon frequency will have its own receiver. Even though a single antenna could be used, the system will be implemented more easily if three independent one meter diameter antennas are used.

Given the low satellite EIRP, the receivers will require very narrow noise bandwidths if large signal fadings are to be measured. This implies the use of frequency or phase control loops locked to highly stable reference signals, to compensate for the drifts in both the local oscillators and beacon generator, and maintain the signal frequencies within the narrow bands of the noise limiting filters (typically in the order of tens of hertzs).

To reduce the receiver complexity we have not considered in principle the implementation in the 20 GHz channel of a synchronous switch locked

---

[1] E.S.A. "Olympus Users' Guide", UG-6-1, Part.1, Propagation Package, Issue 2, November 1983.

to the 933 Hz polarization switched signal radiated by the satellite |1|. For that reason 3 dB will be lost in the dynamic range of that channel |2|.

The main receiver desing criteria will be:

- Large dynamic range. This will impose reduced noise bandwidths.
- Simplicity. The number of frequency conversions should be minimized.
- Reliability. In some way related to the preceding aspect in the sense that implies simple solutions. But high gain stability in the amplifiers and high frequency stability in the local oscillators will be required.

An additional consideration on the final configuration will be the degree of upgrading required, in order to expand during the experiment lifetime the simple attenuation measurements. This means a compromise solution with the above stated simplicity.

RECEIVER CONFIGURATION

The beacon frequencies are obtained from a reference signal - f_B = 290.741 MHz by frequency multiplication. This fact suggests two different design philosophies that are next presented and discussed.

OPTION A. Its principles of operation are illustrated in figure 1, the main feature being the use of the same intermediate frequency (IF) in all three receivers. This greatly simplifies the design since, after the first down conversion, all circuits will be identical. Further simplification results if that frequency is also a multiple of f_B; the first local oscillator (LO) may then be obtained from a single source of that frequency by multiplication. To compensate for the frequency drifts, it will be needed before filtering the noise a phase lock loop (PLL), followed then by the filter or the synchronous detector.

|2| H.W. Arnold, D.C. Cox, H.H. Hoffman, R.H. Brandt, R.P. Leck, M.F. Wazowicz, "The 19 and 28 GHz Receiving Electronics for the Crawford Hill Comstar Beacon Propagation Experiment". The Bell Syst. Tech. Jour. 57, 5, May-June 1978, pp. 1289-1329.

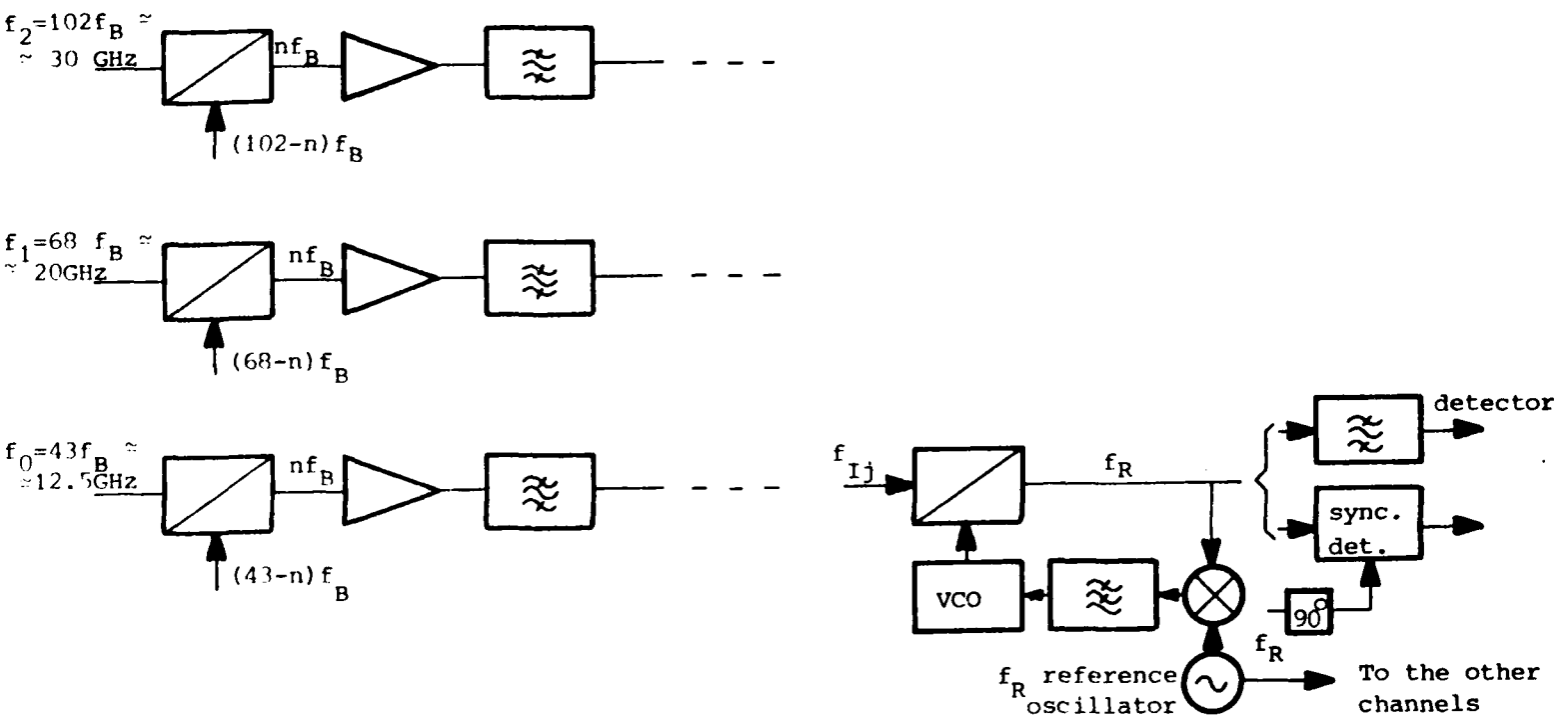

Figure 1. Option A receiver principles of operation

OPTION B. The prominent characteristic of this configuration, as shown in figure 2, is that all intermediate frequencies maintain the same beacon frequency ratio[2]. In this way if all local oscillators, corresponding to the same conversion level in all three channels, are derived from a single source, it will be possible with a single phase lock loop in only one of the channels, to follow in the other two the beacons and local oscillators fluctuations.

As indicated, option A has the advantage of a reduced design cost. The local oscillators of the same mixing level, except the first ones, are identical in all three channels and may be obtained by power division from a single source. The use of synchronous detection may facilitate the solution of the filtering problem. An inconvenience of this configuration is the limitation in the dynamic range of attenuation measurements at 20/30 GHz, imposed by the minimum signal to noise (S/N) required to avoid loss of lock in the phase loops.

Option B may produce a larger dynamic range in those upper channels if the phase lock loop is implemented in the 12.5 GHz channel, where signal fadings caused by hydrometeors will be much lower. On the other hand, starting with this configuration will make easier to expand the system to cover the totality of possible measurements, especially the inter-channel differential phase measurement. But the receiver complexity would be higher than in the other option, and it is not possible to implement the synchronous detector alternative without handicapping the better dynamic range, making unavoidable noise filtering at the last IF.

The down link budgets for the three Olympus beacon receivers according to option B are shown in Table 1. The indicated dynamic ranges correspond to a 50 Hz noise bandwidth [1]. This is a resonable trade-off on the loop bandwidth, considering dynamic range and tracking speed. It is implicitly assumed that under the deepest signal fadings at 20/30 GHz, the 12.5 GHz channel is still above threshold. This last is fixed by the minimum S/N required to maintain locked the PLL, value that has been set at 10 dB [1]. If the option A receiver were used with the same loss of lock criterium, the dynamic ranges at 20/30 GHz shown in Table 1 should be reduced by 10 dB.

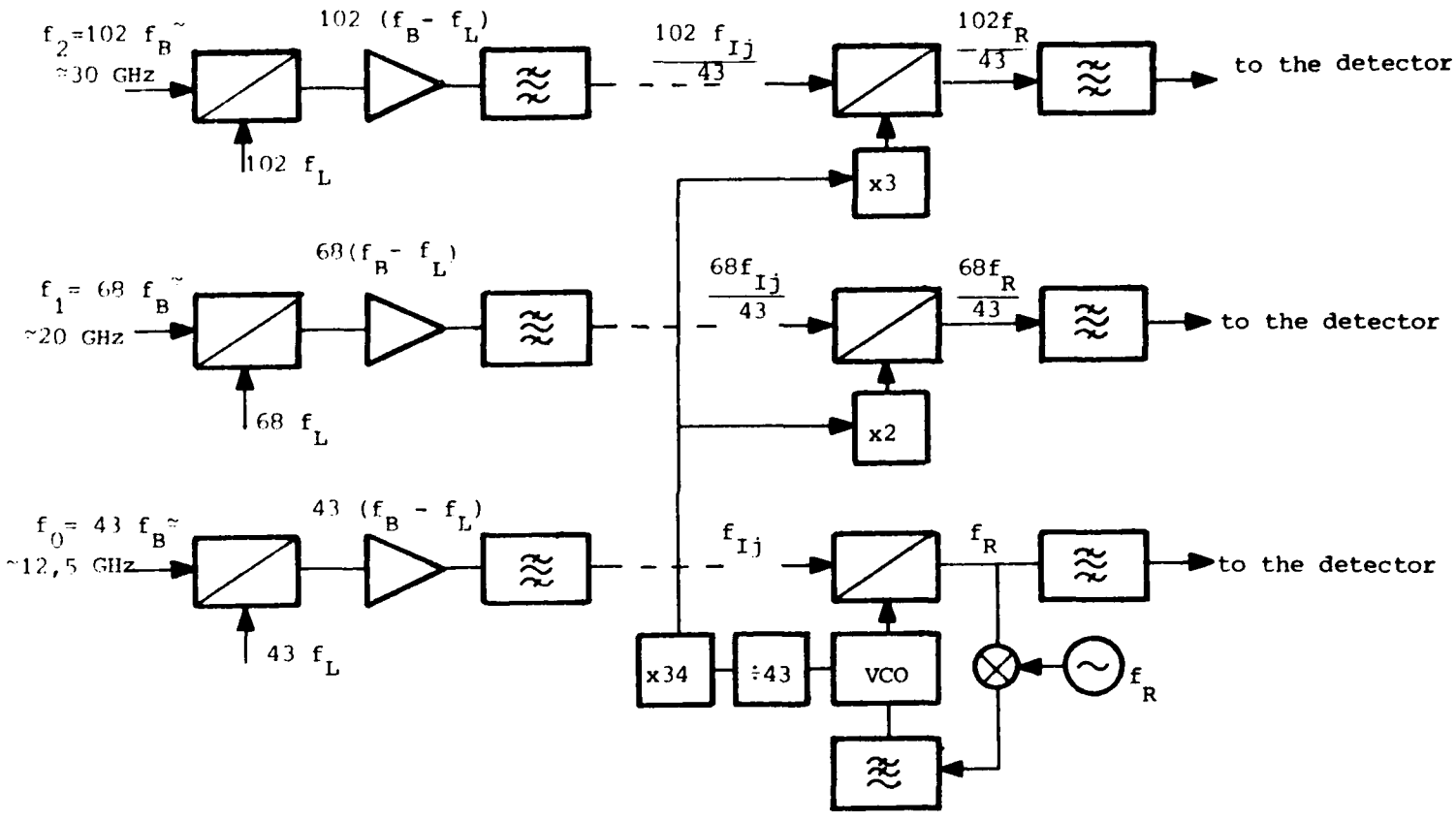

Figure 2. Option B receiver principles of operation.

T A B L E 1

Link budgets for Olympus beacons (cont'd on next page)

	12,5 GHz			20 GHz		30 GHz
	(1,2,3,4)	(1,3,4,5)	(3,4,5,6)	{3,6,7 / 8,9,}	{3,6, / 8,9}	(3,6,9,10)
EIRP (dBW)	10	10	10	24	24	24
Free space path loss (38,000 Km) (dB)	-206	-206	-206	-210	-210	-213.6
Receiving antenna gain (Ø 1m) (dB)	40.1	40.1	39.3	43.4	43.4	46.9
Polarization switching (dB)	0	0	0	-3	0	0
No switching in the receiver (dB)	0	0	0	-3	0	0
Receiver noise temperature (dB)	-29	-33.6	-33.6	-34.6	-34,6	-35.6
Noise bandwidth (50 Hz) (dB)	-17	-17	-17	-17	-17	-17
Boltzmann's constant (dB	228.6	228.6	228.6	228.6	228.6	228.6
C/N (dB)	27.7	22.1	21.3	28.4	34.4	33.3
Measurement dynamic range (dB)	17	12.1	11.3	28	34	33

TABLE 1

Notes (cont'd)

(1) 60% antenna efficiency.

(2) 3.5 dB intrinsic noise figure of the receiver by using a low-noise amplifier.

(3) 290 K antenna temperature included in total noise temperature of the receiver.

(4) Dynamic range to 10 dB S/N loss of lock.

(5) 9 dB intrinsic noise figure of the receiver by direct mixing.

(6) 50% antenna efficiency.

(7) Eventual beacon polarization switching.

(8) 10 dB intrinsic noise figure of the receiver by direct mixing.

(9) Dynamic range to 0 dB S/N.

(10) 11 dB intrinsic noise figure of the receiver by direct mixing.

Block diagrams of both options are represented in figures 3, 4, with approximate values of intermediate frequencies indicated. For the local oscillators frequency assignements of figure 3 (option A), it has been assumed that all are synthesized from a reference signal f_R equal to $f_B/60$, although this is not an essential requirement in the receiver's design. In the option B diagram of figure 4 it has been attempted to minimize the values of the IF's in order to obtain last intermediate frequency values of a few hundred hertz (that will facilitate filtering with 50 Hz or lower bandwidths) with the minimum number of down convertions.

In both cases a first IF has to be selected that will permit construction of a very low noise amplifier. Also in the 20 GHz channel the sidebands produced by the polarization switching will have to be discriminated. This will be achived by filtering in option B and locking on the carrier the 20 GHz channel PLL in option A.

It is also evident in both cases that, in order to maintain the maximum dynamic range, the first mixer, that will be of a Schottky diode balanced type, and at least the first IF amplifier stages, should be mounted on the antenna feed.

It should be noted that the frequencies indicated in figures 3 and 4 will have to be revised taking into account the availability of certain components - frequency multipliers and divisors, oven controlled crystal oscillators, voltage controlled oscillators, etc. and the practical feasibility of filtering image frequencies close to the signal. Also important details as capability of calibration signal injection, the presence of precission attenuators for level adjustments, or the inclusion of automatic frequency control circuits before the PLL, have not been represented in the block diagrams.

The frequency stability requeriments imposed by the output narrowband filters and the coherence of local oscillators of the same mixing level, in option B, advise the synthesis of the local oscillators by multiplication of highly stable crystal oscillators. Nevertheless other choices, like subharmonic synchronization of the first local oscillators with a stable reference, may be considered.

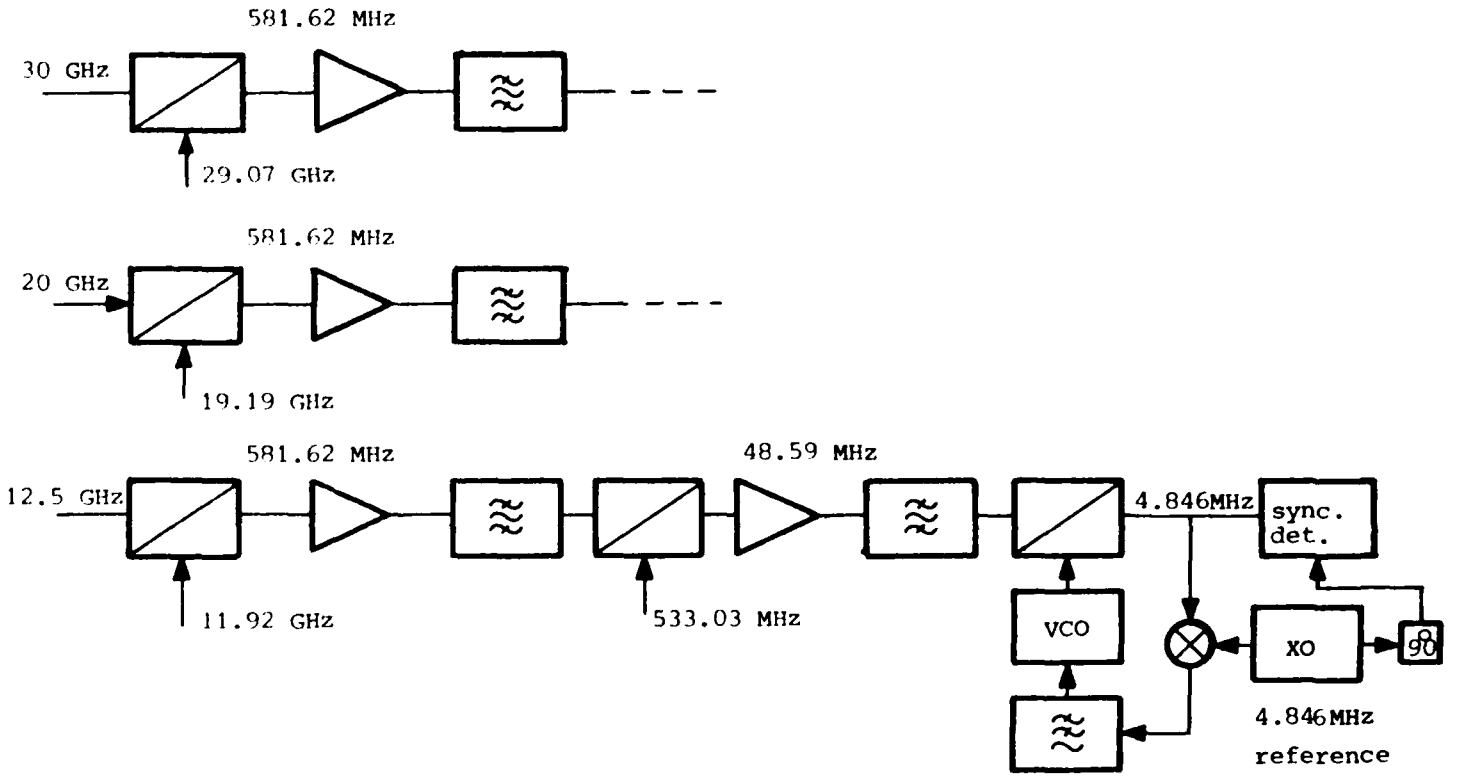

Figure 3. Option A block diagram

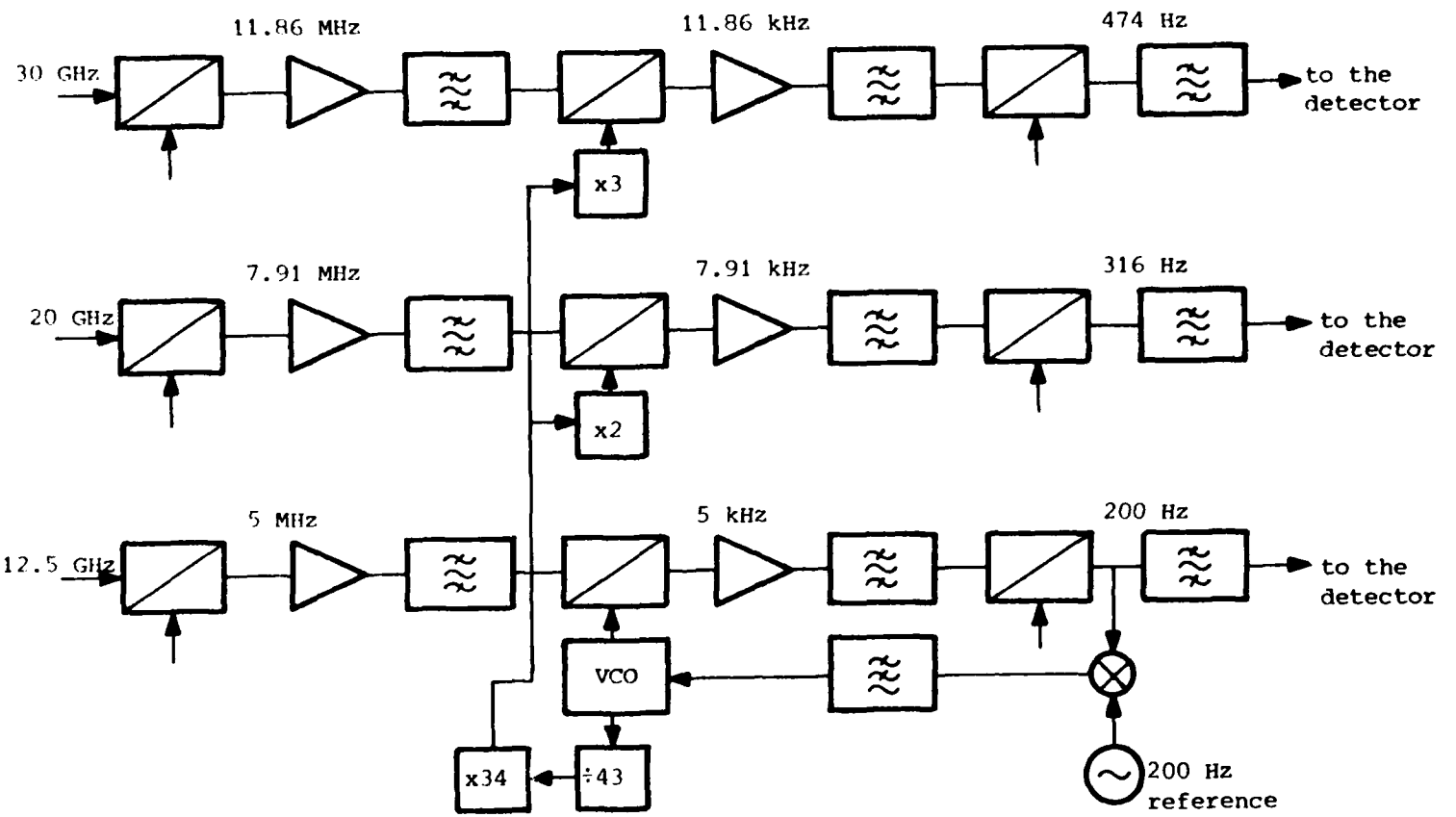

Figure 4. Option B block diagram

3. SCALAR AND VECTOR MEASUREMENT SYSTEMS

The development of 20/30 GHz subsystems require the setting of amplitude and phase measurement systems, both in reflexion and transmission modes. The operating options available in our laboratory, 2 - 20 GHz automatic vector system, 36 GHz manual scalar for reflection and transmission measurements, and a vector reflection set up at the same frequency, are described in the following paragraphs together with those in process of installation.

AUTOMATIC VECTOR SYSTEM

An HP 8408A Automatic Network Analyzer is available, including an HP 8350A generator with HP 83590A 2 - 20 GHz RF plug-in. The receiver of this analyzer is the model 8411A (option 018), specified up to 18 GHz with an equivalent maximum noise at the test-port input of -68 dBm. Nevertheless this system may be used at 20 GHz with less performance, due to the noise degradation at the input.

SCALAR SYSTEM

The laboratory equipment in Ka-band includes a WR-28 bench for reflection and transmission scalar measurements in the 35.8 to 36.2 GHz frequency range, with the block diagram shown in figure 5. It includes a Hughes 47271H - 211(varactor tuned Gunn diode oscillator.

Reflection measurements are performed calibrating with a short circuit and reading the attenuator difference when the device under test is inserted, yielding the device return loss. In the transmission mode the insertion loss is measured calibrating first without the device and adjusting then the variable precision attenuator to obtain the same detected signal when the device is inserted.

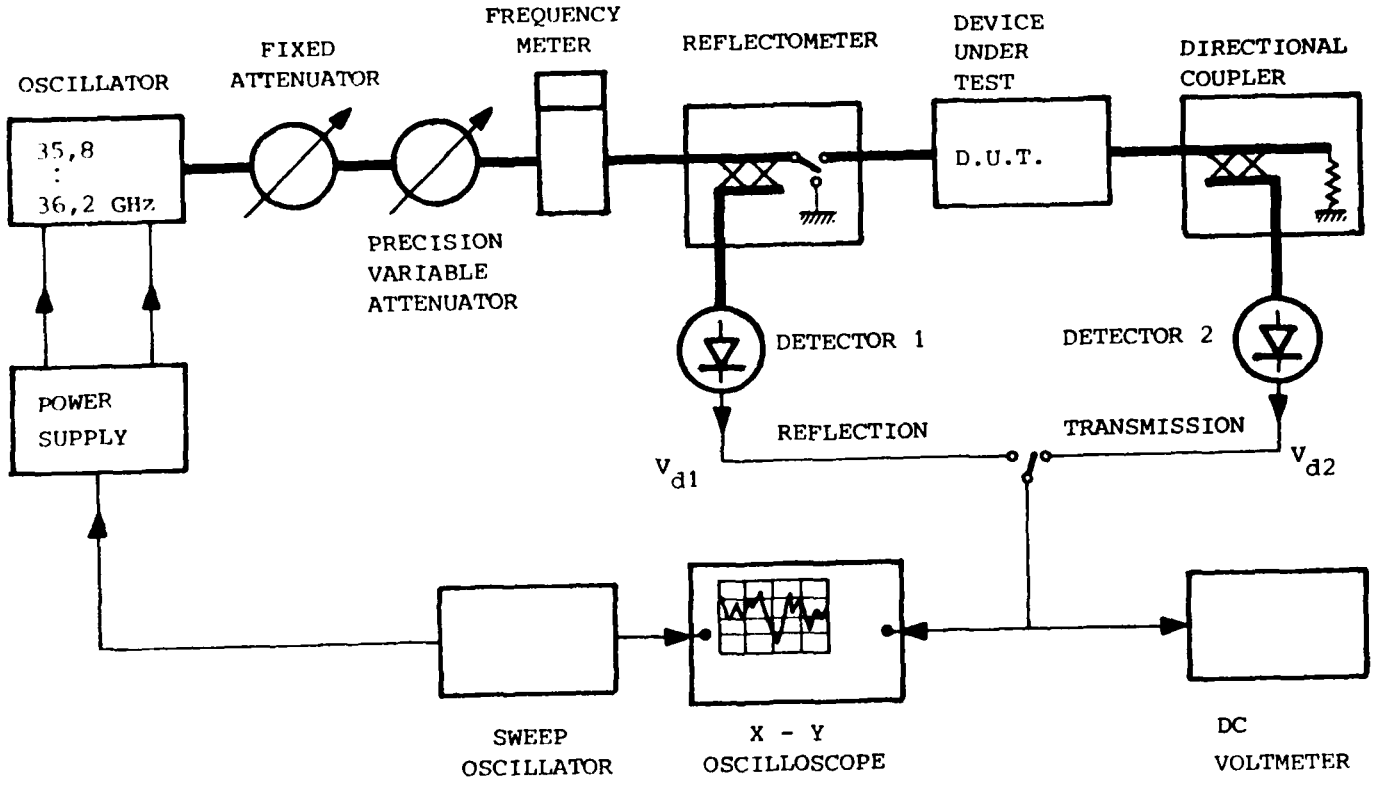

Figure 5. K_a-band scalar measurement system. Reflection and Transmission

VECTOR SYSTEM

Using a waveguide magic-tee impedances may be measured. The system operates as an impedance bridge, where two magic-tee access have to be balanced with equal impedances: one is the unknown, and the other one known and synthesized with an attenuator and phase shifter, figure 6.

Different loads have been measured at 36 GHz using this system. A set of diaphragms was constructed by photoetching and chemical attack of 0.15 mm copper sheets and measured. The results are plotted in figure 7 together with their theorical values [3]. One of the main limitations of the system is that impedance balance is achieved when V_d in figure 6 becomes zero, so that the system's sensitivity is limited by the noise at the output of the detector, On the other hand only pasive devices can be measured with this procedure.

To make measurements over the full K_a-band (26,5-40 GHz) a system based on the one presented by J. Paul [4] was chosen and is in the process of installation. It will allow the use of the waveguide (WR-28) devices available in the laboratory and convertion of the scalar bench to a vector system. Figure 8 shows the reflection and transmission system's block diagrams.

In the reflection mode, calibration is done by placing a short-circuit in the position of the device under test (DUT), adjusting the attenuators and phase shifter to produce a null reading in the detector's output; after insertion of the DUT, the attenuator and phase shifter in the test arm have to be adjusted to restore the null. The difference in the attenuator readings (RL) gives the return loss in dB, and together with the phase shifter difference $\Delta\phi$ yields the reflection's coefficient module and phase:

$$|\Gamma| = 10^{-(RL)/20} \quad , \quad \angle\Gamma = \Gamma - \Delta\phi$$

---

[3] N. Marcuvitz, "Waveguide Handbook". Mc Graw-Hill, 1951.

[4] J. A. Paul, "Wideband Millimeter-Wave Impedance Measurements". Microwave Journal, April 1983, pp. 95-102.

In the transmission mode, calibration is done replacing the DUT by a waveguide section and adjusting attenuators and phase shifter for zero detector output. After insertion of the DUT, the reflection coefficient is found following the procedures above indicated.

The use of sincronous detection gives much better sensitivity in the null readings. For that purpose the oscillator signal is modulated in amplitude by an square wave produced by a pin-modulator. The design of this modulator is well advanced, using the waveguide to fin-line tapers presented in a latter section.

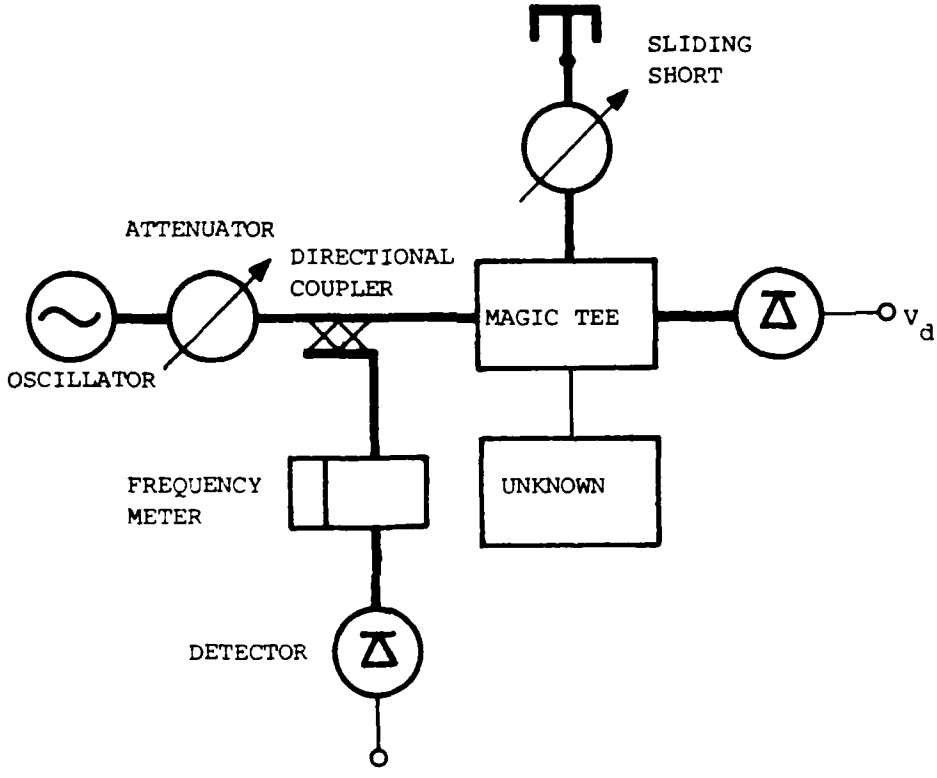

Figure 6. K_a-band vector measurement system. Reflection

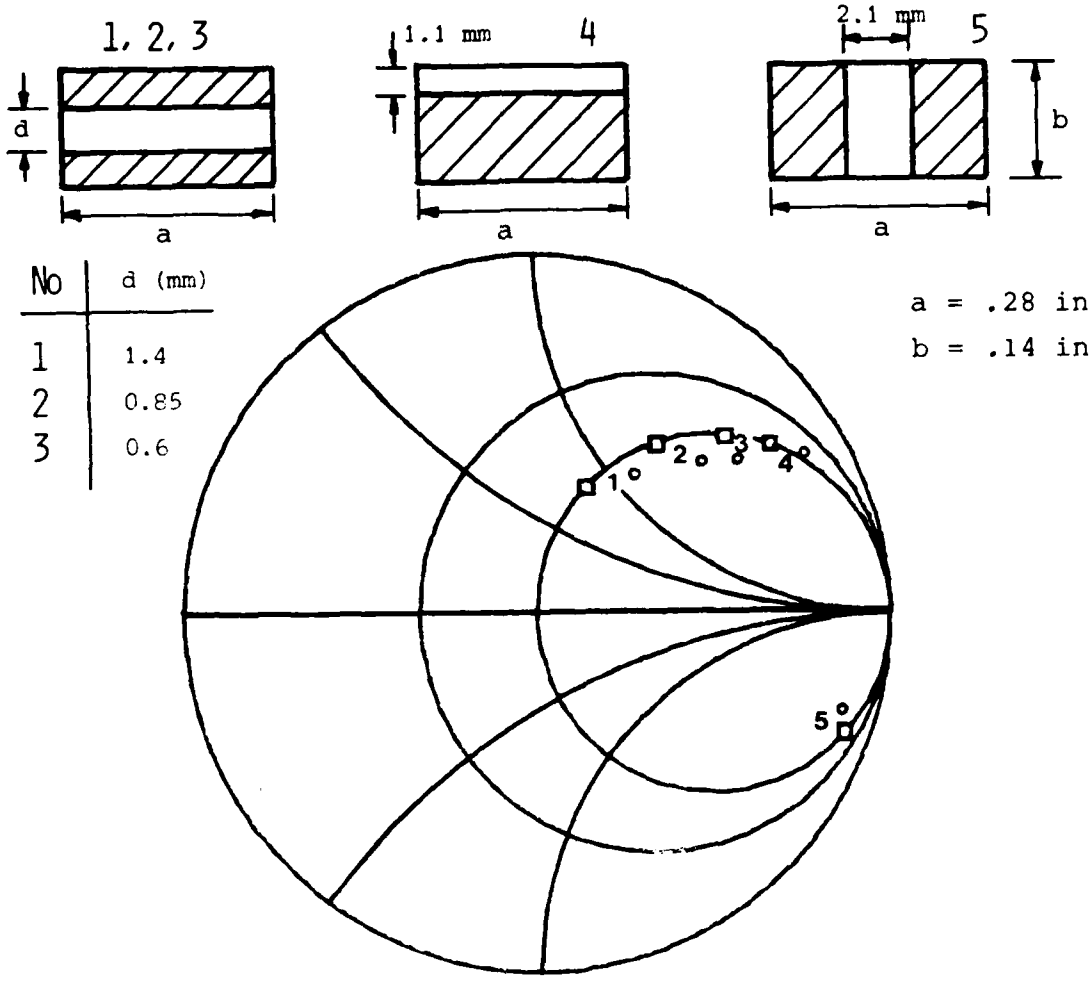

Figure 7. Theoretical (◘) and experimental (e) iris admittances measured with an adapted waveguide load.

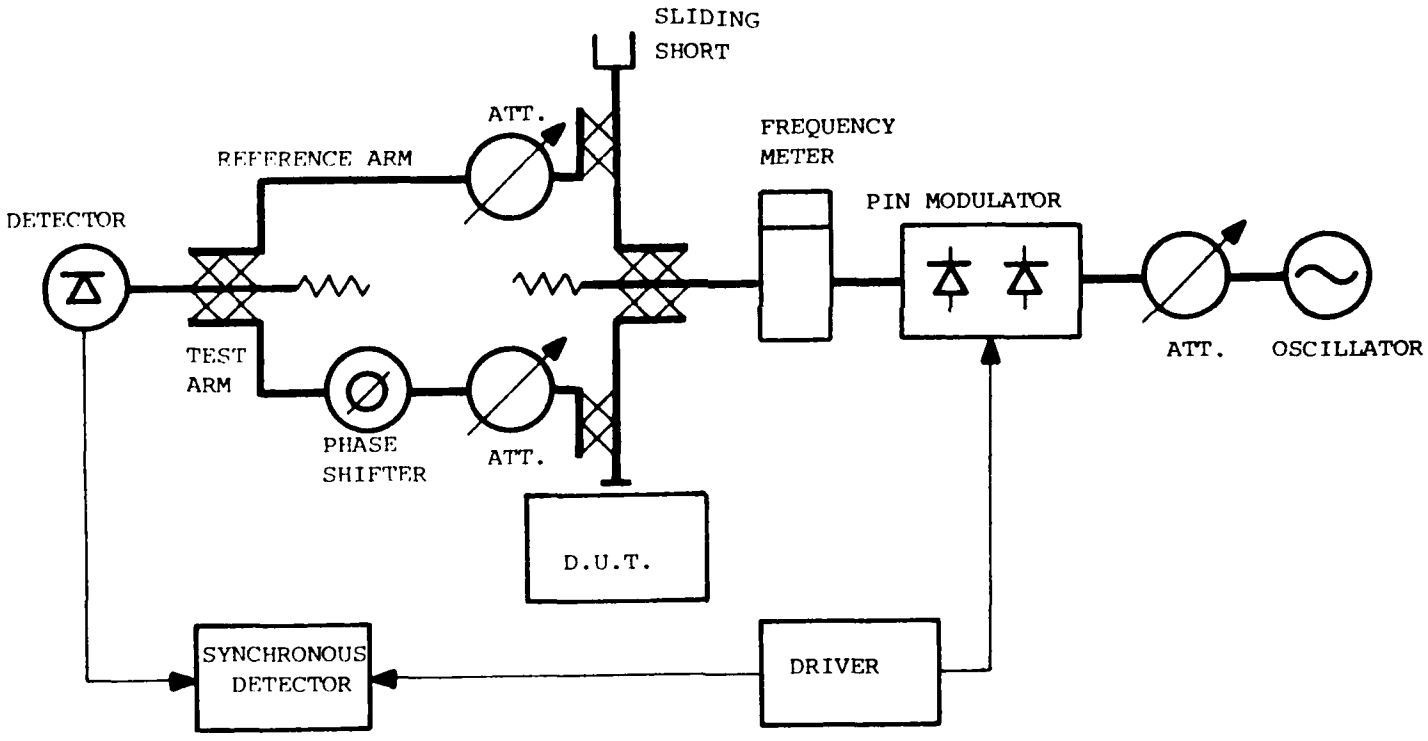

Figure 8a. K_a-band reflection vector measurement system.

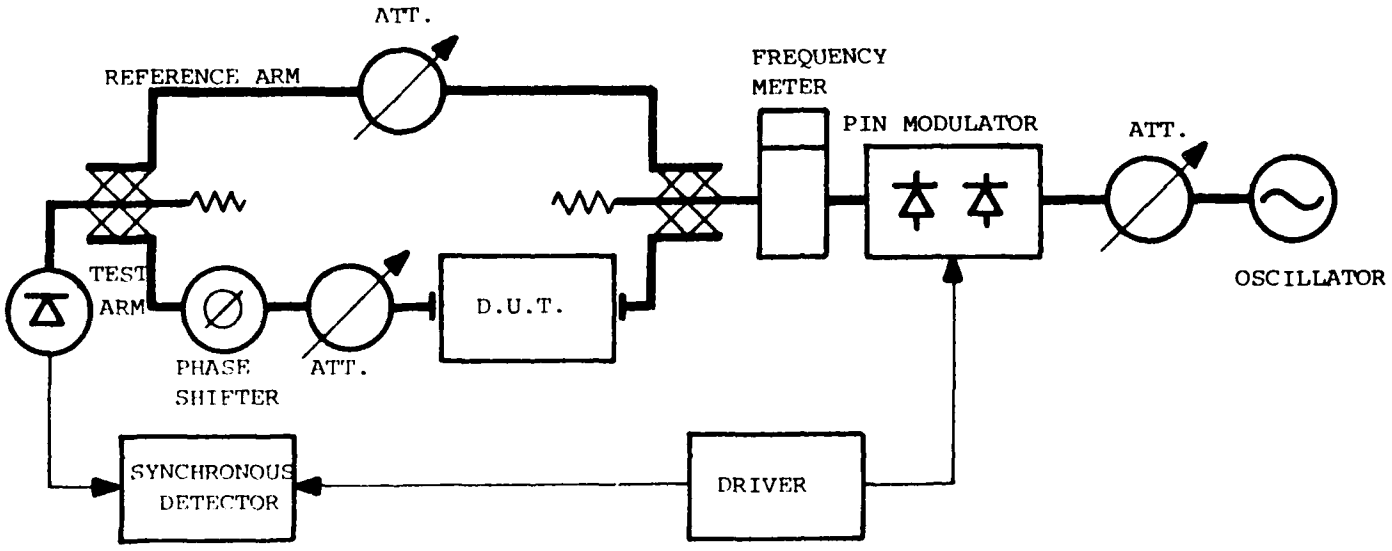

Figure 8b. K_a-band transmission vector measurement system.

4. GUNN DIODE OSCILLATORS

Two K_a-band waveguide mounted gunn diode oscillator prototypes have been constructed. A 36 GHz operating frequency was selected, due to initial measurement equipment limitations. Both desings use a rectangular waveguide post mounted gunn diode type AH604, manufactured by Thomson-CSF. In the first one the cavity was constructed using standard WR-28 waveguide. Its performance was analysed using a simplified equivalent circuit and compared with measurements. Some effects as frequency saturation and frequency jumps in the mechanical tuning characteristics were present. The second design uses a reduced height waveguide with quarter-wavelength transformers, having disappeared the above effects.

STANDARD WAVEGUIDE OSCILLATOR

The design of a gunn diode oscillator requires a knowledge of its impedance or the equivalent or the equivalent circuit. Usually those characteristics are not given by the manufacturer and an impedance measurement, in large signal if possible, is in general required. If the exact values of the diode impedance are not known a priori, the design must include sufficient degrees of adjustment to optimize the characteristics of the oscillator.

The structure selected is shown in figure 9. Since the diode is a low impedance device, the design of the cavity may be done, in a first approximation, assuming the diode is not present and the post extends from wall to wall [5]. In this way the cavity dimensions (ℓ_1, ℓ_2) and the iris susceptance B_i may be obtained. The frequency behaviour of the oscillator is found by imposing a resonance condition in the equivalent circuit shown in figure 9.

$$\frac{B_i + \operatorname{tg} \beta\ell_1}{1 - B_i \operatorname{tg} \beta\ell_1} + B_p - \operatorname{ctg} \beta\ell_2 = 0$$

---

5 J.F. White, "Simplified Theory for Post Coupling Gunn Diodes to Waveguide". IEEE Trans. on MTT-20, June 1972, pp. 372-378.

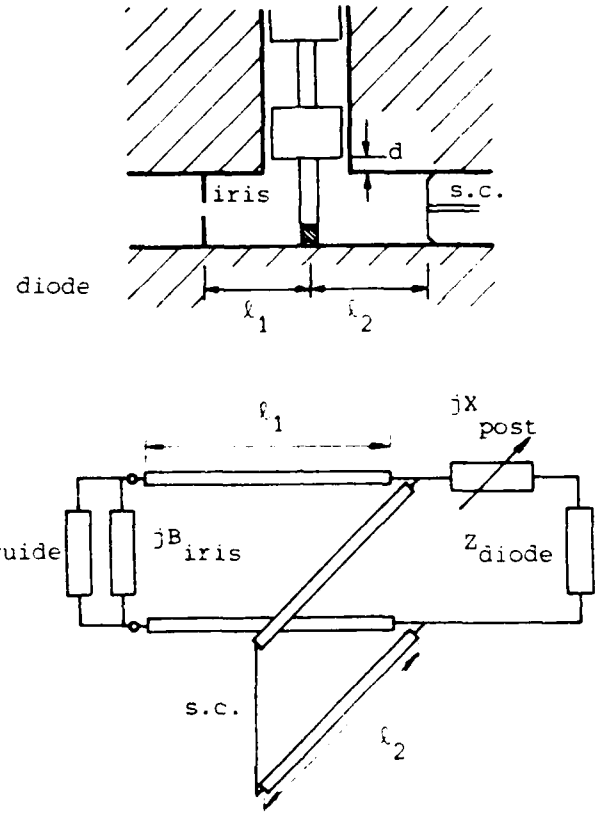

Figure 9. Gunn diode oscillator and equivalent circuit.

with B_p the post susceptance and β the propagation constant.

The mechanical appearance of the oscillator is shown in figure 10, the two pieces forming an standard WR-28 waveguide. The U-part contains a coaxial low pass filter (quarter wavelength sections) for biasing the diode. The coaxial inner conductor is isolated from its surroundings by a 0.1 mm teflon ribbon. The diode is threaded in the U cover, and to insure good contact with the post, a polyethylene cylinder acting as an spring is placed under the conector. The total length of the waveguide section is less than a wavelength.

The frequency of oscillation and the power output are shown in figure 11a for different short circuit lengths ℓ_2 (ℓ_1 fixed and $d = 0$). The following phenomena appear crearly: The tuning range is relatively narrow and is displaced towards the lower frequencies. Frequency jumps are present and there are unstable oscillation areas related to resonances not considered in the simplified equivalent circuit. Also a frequency saturation effect [6] is shown, due to the appearance of local resonances between the upper and lower waveguide walls created by the post and the diode's packaging.

This last effect may be eliminated reducing the guide height or elevating the diode over the lower wall, for instance by placing it in the middle of the post. In all cases one tries to increase the local resonance frequency and bring it out of the frequency range of interest. Figure 11b shows the effect of elevating the diode on a 0.3 mm metalic pedestal; compared with the other case, an increase in the tuning range and a shift towards the upper frequencies have been obtained.

From the oscillation circuit analysis it may be deduced the diode presents an inductive reactance, attributed to packaging effects since the diode has an intrinsic capacitive characteristic. This result is in agre-

---

[6] B.C. Taylor, S.G. Fray, S.F. Gibs, "Frequency-Saturation Effects in Transferred Electron Oscillators". IEEE Trans. on MTT-18, November, 1970, pp. 799-807.

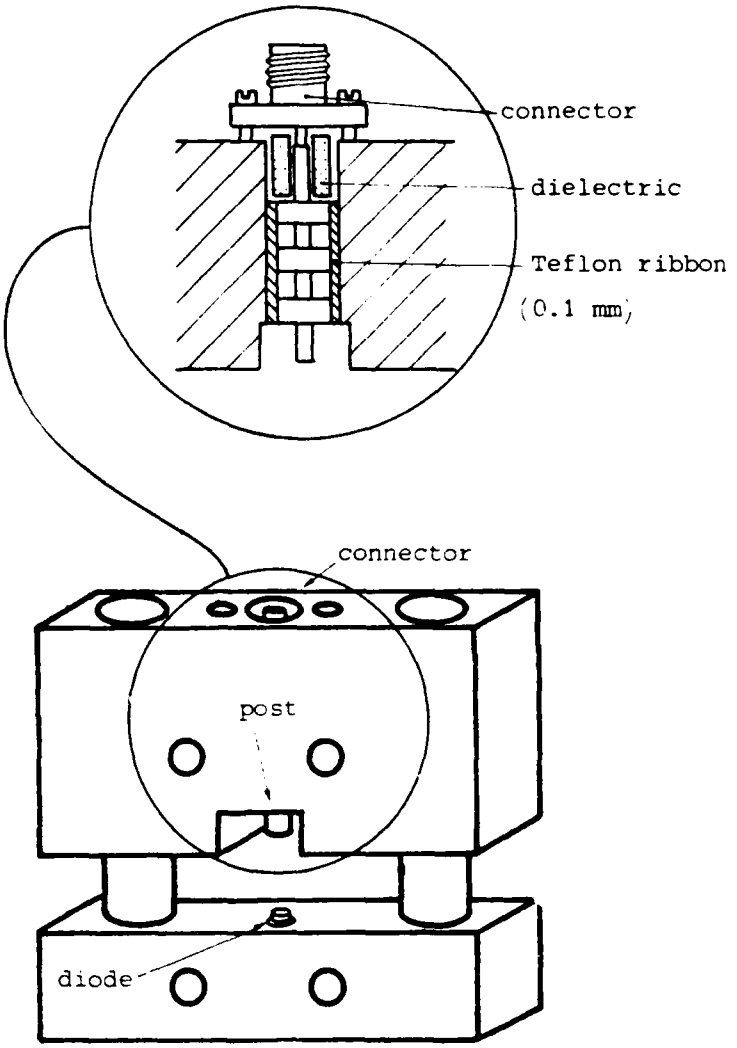

Figure 10. Mechanical configuration of Gunn diode oscillators.

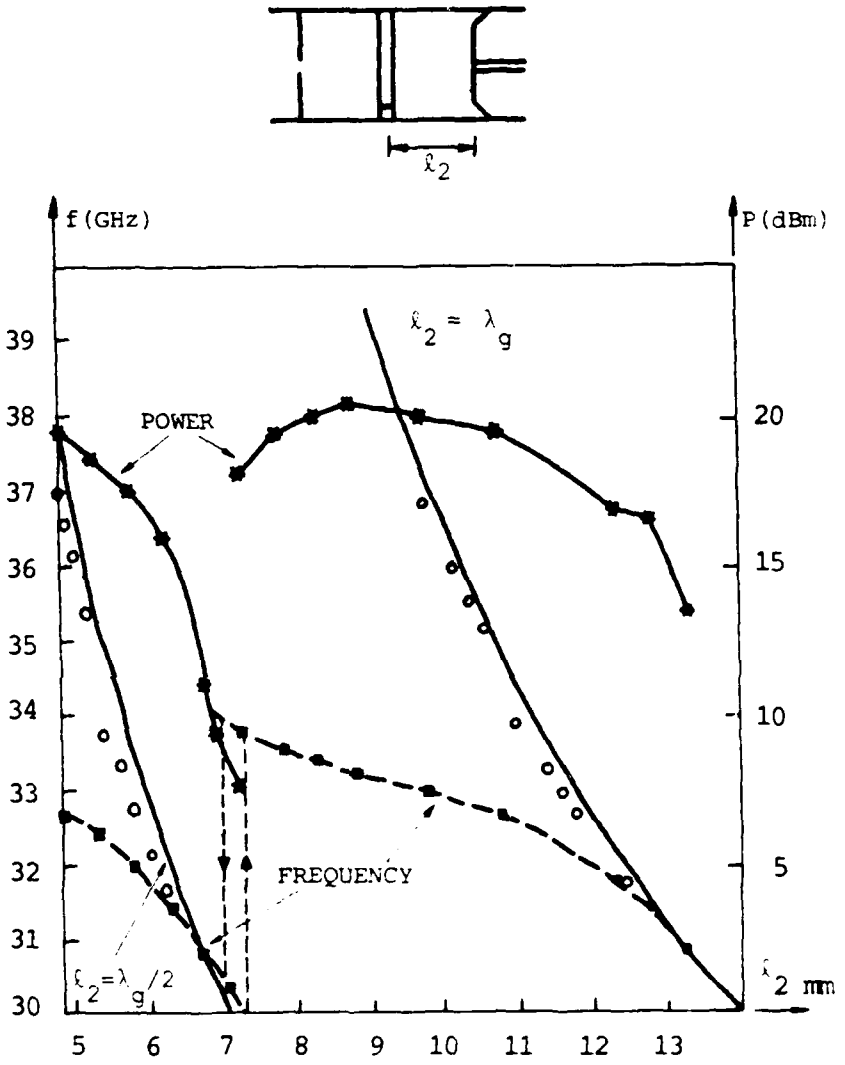

Figure 11a. Gunn diode oscillator frequency and power output.
(*) Measured power. (■) Measured frequency.
(o) Calculated frequency

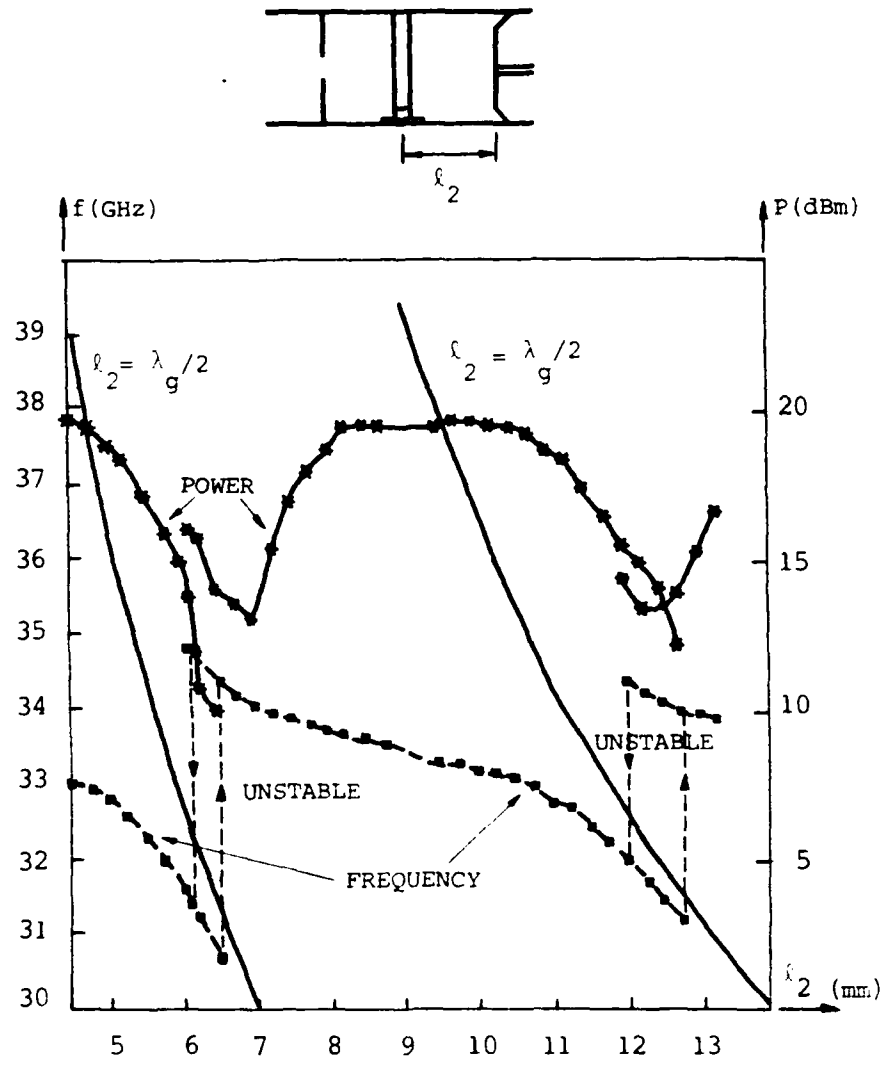

Figure 11b. Gunn diode oscillator frequency and power output (diode mounted on pedestal). (★) Measured power. (■) Measured frequency

ement with published data [7]

REDUCED HEIGHT WAVEGUIDE OSCILLATOR AND TRANSFORMER

To avoid the described frequency saturation problems a reduced height waveguide oscillator was built with the configuration and equivalent circuit [8] shown in figure 12. It has the advantange that both the real and imaginary part of the load impedance Z_L presented by the diode may be adjusted. This impedance is given by

$$Z_L = \frac{Y_o}{Y_o^2 + B_s^2} + j\left(X_{coax} - \frac{B_s}{Y_o^2 + B_s^2}\right)$$

the admitance towards the output waveguide, Y_o is fixed by the transformation ratio R; the coaxial section, placed between the dc-bias filter and the diode, contributes a reactance X_{coax}; and the short circuit presents, in the diode's reference plane, a susceptance B_s.

The mechanical design was similar to the one shown in figure 10. A two section quarter wavelength waveguide transformer was added with a transformation ratio of 3 and its design included consideration of the discontinuities reactances [9].

The results of the frequency and power measurements are shown in figure 13, where it is observed the small dependence of both with the susceptance B_s. It appears again that the frequency of oscillation is fixed by the coaxial resonance, and its adjustment may be done varying the length d of the coaxial cavity.

---

[7] J.G. Konning et al. "Gunn-Effect Amplifiers for Microwave Communication Systems in X, K_u and K_a Bands". IEEE Trans. on MTT-23, April 1975, pp. 367-374.

[8] H.J. Kuno, "Solid State Millimeter-Wave Power Sources and Combiners". Microwave Journal, June 1981, pp. 21-34.

[9] Mathaei, Young, Jones, "Microwave Filters, Impedance-Matching Networks and Coupling Structures". Mc Graw-Hill, 1964.

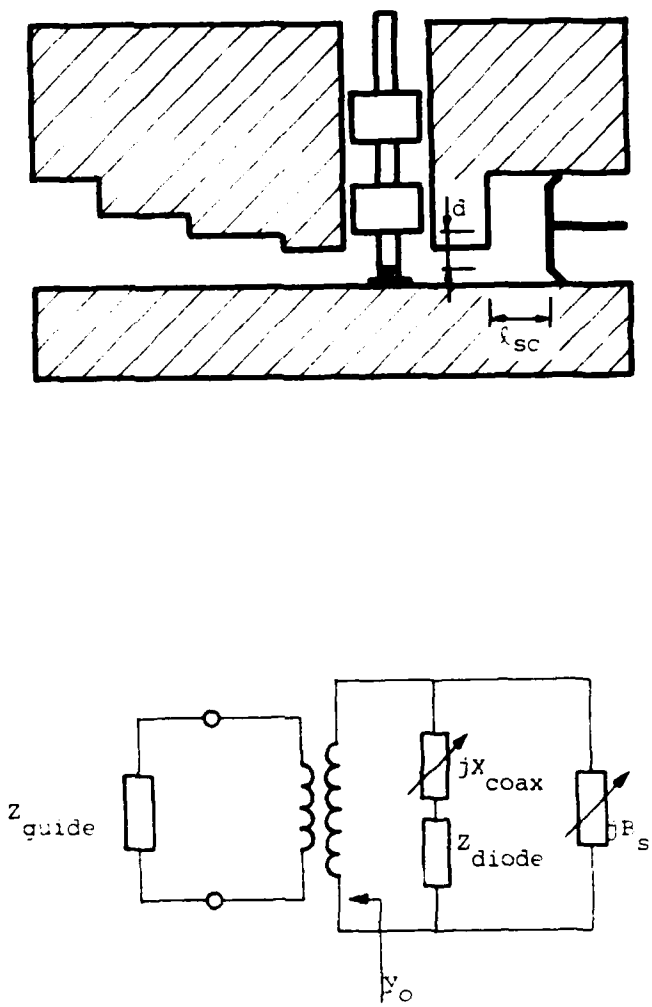

Figure 12. Reduced height waveguide Gunn diode oscillator.

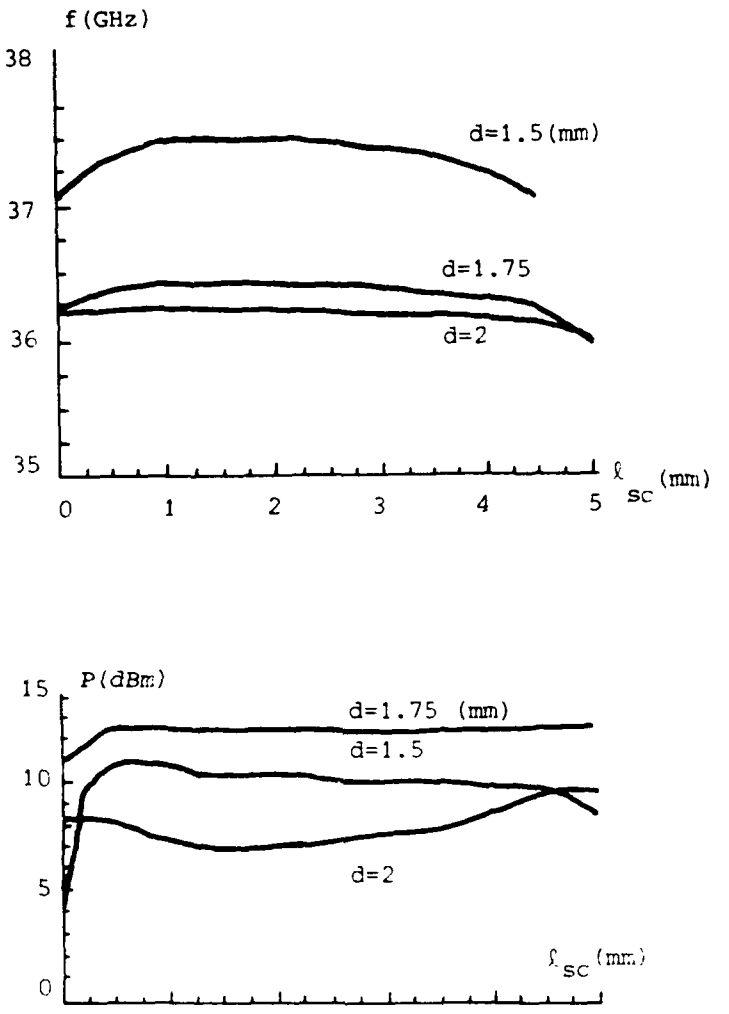

Fugre 13. Frequency and power output of reduced height waveguide Gunn diode oscillator.

In conclusion two oscillator prototypes have been constructed. The first one, using a WR-28 resonant cavity, presented a great simplicity of construction but frequency-saturation effects caused by coaxial resonances. In the second one the coaxial resonator effect has been retained and the waveguide cavity replaced by a tranformer. Two possible adjustments control the frequency and the power output of the oscillator.

5. PASSIVE CIRCUITS.FIN-LINE TRANSITIONS

For the construction of K_a band active and passive circuits on fin-line, design methods based on closed form expressions for the impedance and velocity of propagation on them have been used. An empirical expansion for the unilateral fin-line effective dielectric constant is proposed, in the range where appropriate formulas are not available. Results of various rectangular waveguide to unilateral fin-line tapers and antipodal fin-line to microstrip transitions, constructed on Duroid 5880 of 0.010" thickness and a dielectric constant value of 2.22, are presented.

ANALYSIS OF UNILATERAL FIN-LINES

The unilateral fin-line structure shown in figure 14 consists of a waveguide loaded in the E-plane with a dielectric substrate on which conductive strips have been deposited.

The line is fully described by the wavelength λg and the characteristic impedance Z_o both function of the geometry and frequency. The pseudo-characteristic impedance has been defined as $Z_o = V_o/I_\ell$, with V_o the voltage across fins, calculated by integration of the electric field along the shortest path, and I_ℓ the total longitudinal current in the line. This definition is very convenient for fin-lines with active devices conected in parallel.

For the analysis of this structure the expressions proposed by Sharma and Hoefer [10] have been used. The values of Z_o and λ_g obtained agree, within 2%, with those found by numerical methods, under the following dimensional restrictions:

$$0.35 < b/\lambda < 0.7 \quad \text{(frequency)}$$

$$1/16 < d/b < 1/4 \quad \text{(slot)}$$

$$1/32 < s/a < 1/4 \quad \text{(substrate)}$$

---

[10] A.K. Sharma, W.J. Hoefer, "Empirical Expressions for Fin-line Desing" IEEE Trans. on MTT-31, April 1983, pp. 350-356.

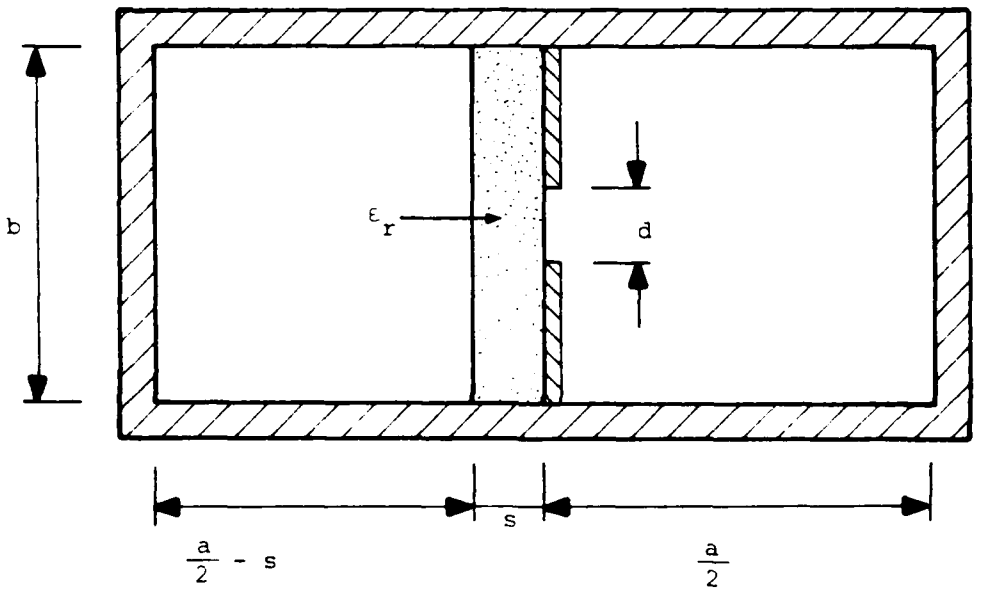

Figure 14. Unilateral fin-line.

The above expressions assume the effective dielectric constant K_e independent of frequency. Two FORTRAN programs have been written, the first one, "FINLINEF", calculates Z_o and λ_g as a function of frequency, and the second one, "FINLINEW" calculates Z_o and λ_g as a function of the slot width. The results obtained are shown in fugures 15-17, and if compared with those found by other methods, like the spectral one [11] the error does not exceed 2.5% in any case.

If a waveguide to fin-line taper is to be constructed, the values of Z_o and λ_g are needed for any slot width d, but the preceding analysis is only valid for $d/b < 0.25$, requiring an extension to the range $0,25 < d/b < 1$ that can be done in the following way.

Using for Z_o and λ_g the expression given by Meier [12]

$$\lambda_g = \frac{\lambda_o}{\sqrt{k_e - (\lambda_o/\lambda_{ca})^2}}$$

$$Z_o = \frac{Z_{o\infty VI}}{\sqrt{k_e - (\lambda_o/\lambda_{ca})^2}}$$

with λ_{ca} and $Z_{o\infty VI}$ the cut-off wavelength and the characteristic impedance at infinite frequency of the ridge waveguide with identical dimensions, respectively. The value of λ_{ca} for $d/b > 0.25$ may be found using expressions given by Hoefer [13] for the ridge guide, valid for $0.01 < d/b < 1$.

The problem then reduces to finding K_e in the range $0.25 < d/b < 1$

---

[11] J.B. Knorr, P.M. Shayda, "Millimter-Wave Fin-line Characteristics". IEEE Trans. on MTT-28, July 1980, pp. 737-743.

[12] P.J. Meier, "Integrated Fin-line Millimiter Components". IEEE Trans. on MTT-22, December 1974, pp. 1209-1216.

[13] W.J. Hoefer, M.N. Burton, "Closed-Form Expressions for the Parameters of Finned and Ridged Waveguide". IEEE Trans. on MTT-30, December 1982, pp. 2190-2194.

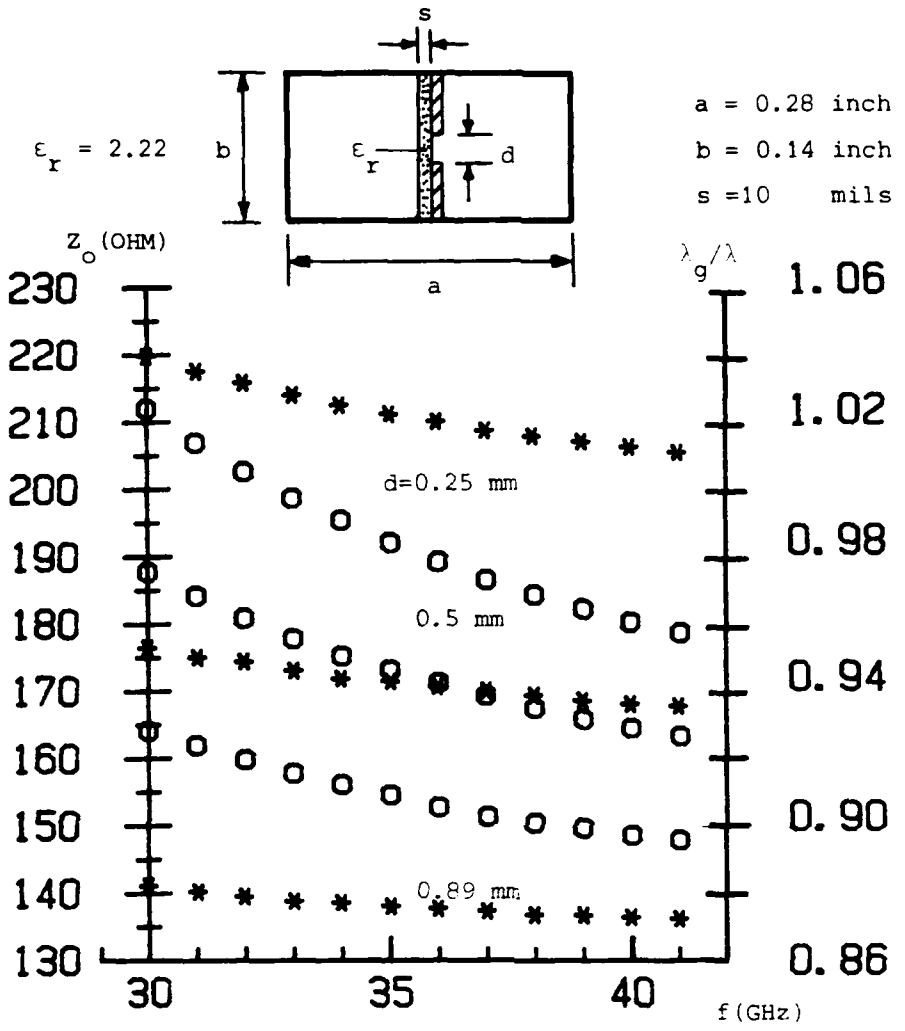

Figure 15. Fin-line impedance Z_o (*) and wavelength λ_g(o), for three different slot widths d.

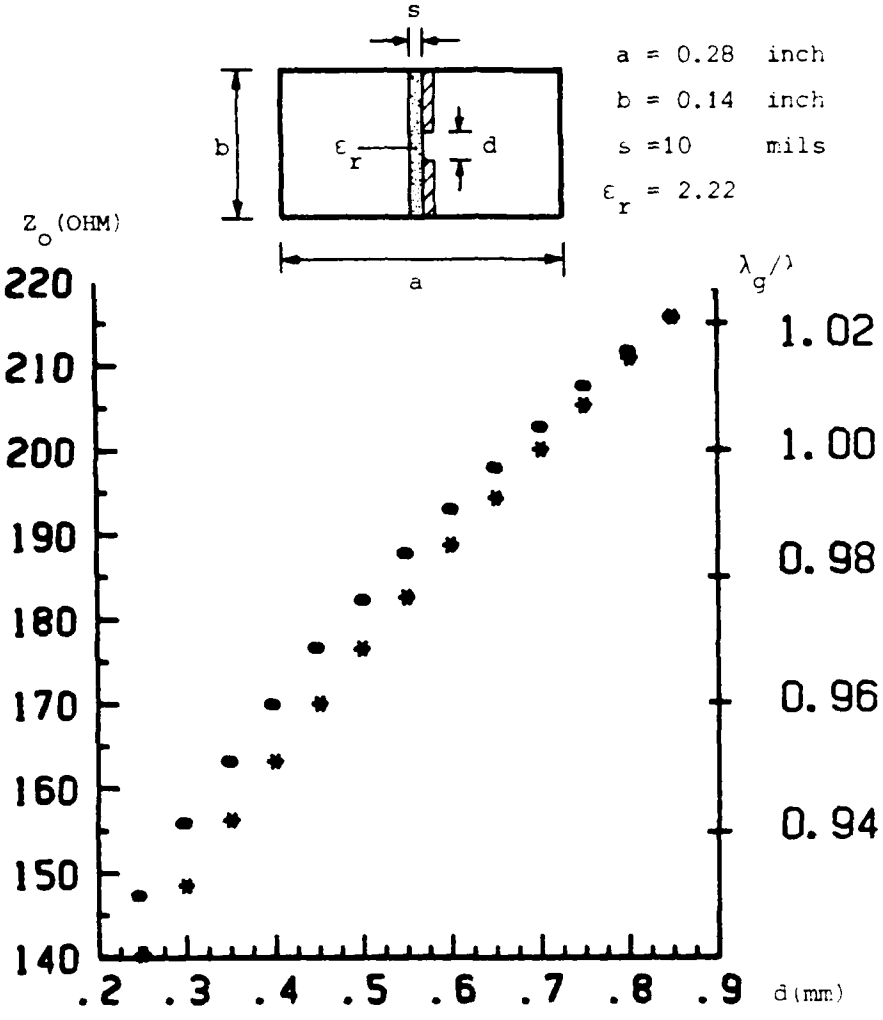

Figure 1c. Fin-line impedance Z_o (*) and wavelength λ_g (●) at 30 GHz, versus slot width d.

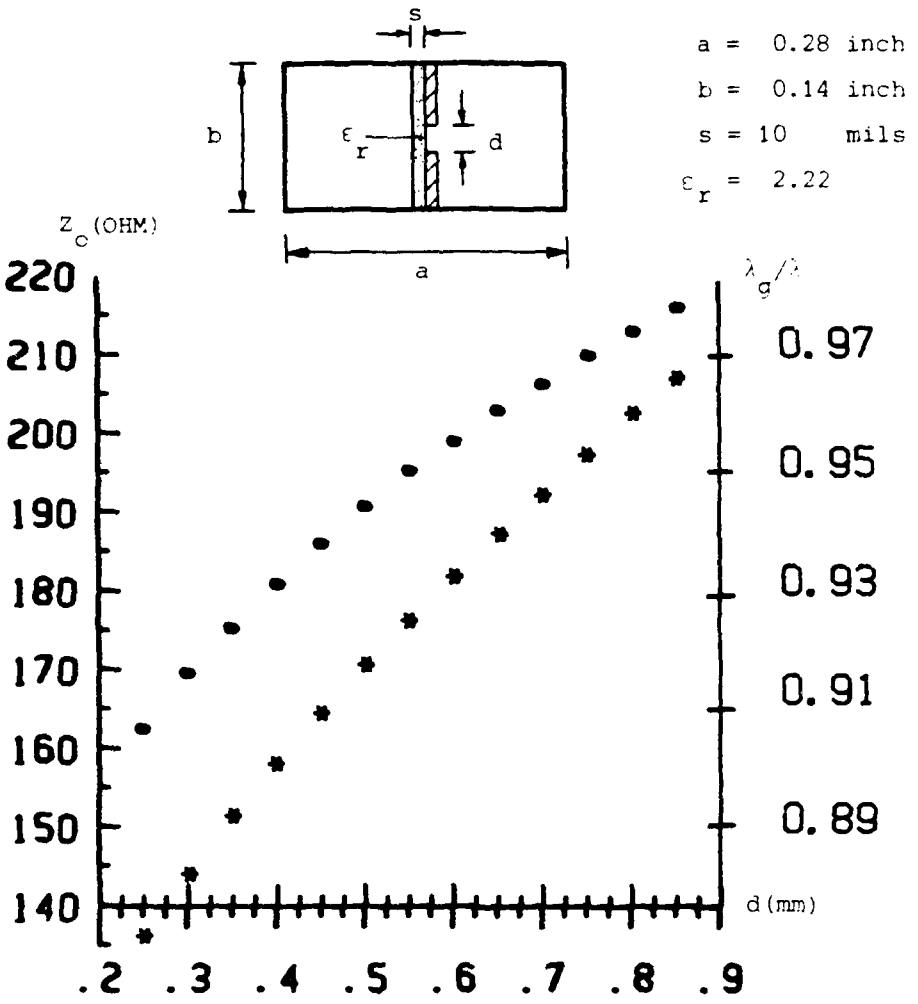

Figure 17. Fin-line impedance Z_o (★) and wavelength (●) at 3[illegible] GHz, versus slot widths d.

When d/b = 1 the fin-line becomes an slab loaded waveguide, that may be solved exactly using a classical transversal resonance method. K_e varies slowly with frequency and it may be assumed constant over the full K_a-band. The following approximation has been used for the effective dielectric constant in the range $1/16 < d/b < 1$

$$K_e = 1.36 - \sqrt{0.07698\ (d/b - 0.0625)}$$

The values obtained using this expression are compared in figure 18 with those using Sharma's [10] and Hoefer's [13] formulations in the range $b/d < 0.25$, and figure 19 shows the values of Z_o versus the slot width.

RECTANGULAR WAVEGUIDE TO UNILATERAL FIN-LINE TRANSITION

Different types of transitions with a continuous impedance taper have been analyzed and constructed. The minimun slot width chosen is 0.3 mm, a value that will allow the mounting of beam lead PIN diodes later on. Two types of taper have been considered, exponential and triangular [14], with an impedance variation along the taper length L given by

$$\bar{Z} = e^{(z/L)\ \ln \bar{Z}_L} \qquad \text{(exponential)}$$

$$\bar{Z} = \begin{cases} e^{\{2(z/L)^2\}\ \ln \bar{Z}_L} & 0 < Z < L/2 \\ e^{\{(4\ z/L) - (2\ z^2/L^2) - 1\}\ \ln \bar{Z}_L} & L/2 < z < L \end{cases} \qquad \text{(triangular)}$$

with $\bar{Z}_L$ the unloaded waveguide normalized impedance and $\bar{Z}$ the tapered fin-line impedance, normalized to the minimum width slot impedance.

Two values of L were chosen, corresponding to 1.5 and 2 times the

---

[14] R.E. Collin, "Foundations for Microwave Engineering". Secc. 5.12 Mc Graw-Hill, 1966.

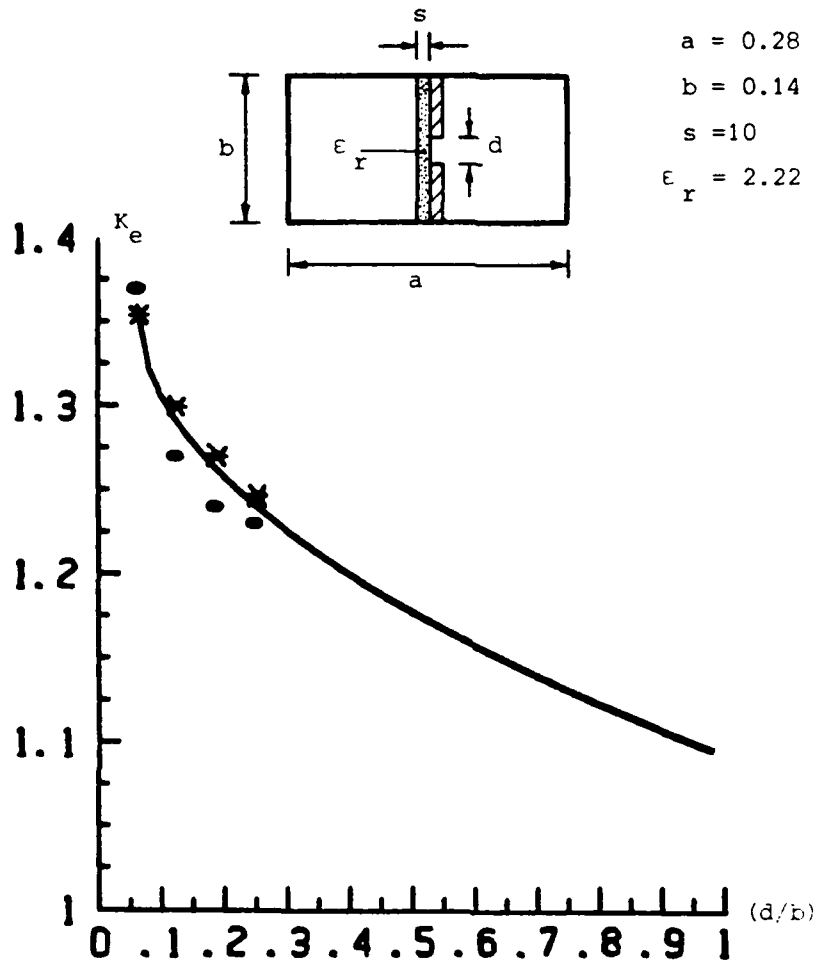

Figure 18. Fin-line effective dielectric constan K_e suggested appoximation. (*) sharma's [10] and (•) Hoefer's [13] values.

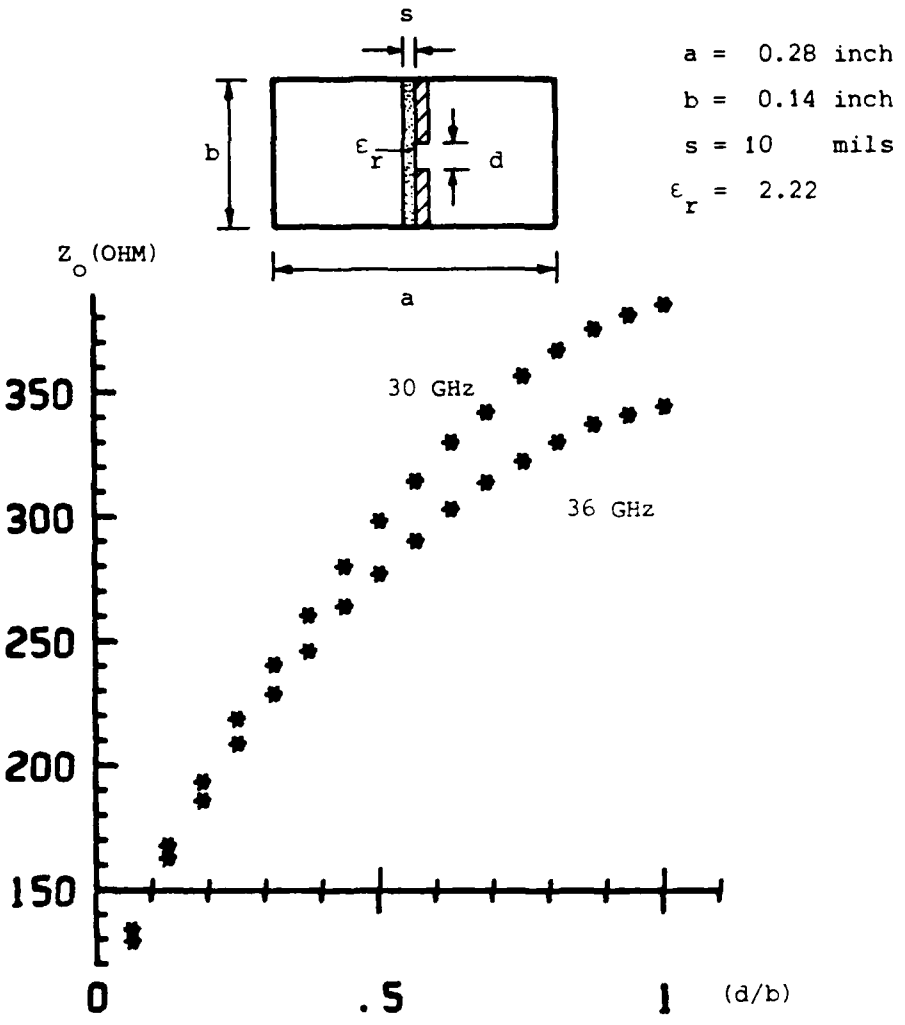

Figra 19. Fin-line impedance.

wavelength of the unloaded waveguide at a frequency of 36 GHz. The circuit masks are shown in figures 20-21, and the transitions have been implemented on 0.010" Duroid 5880 substrate.

The double transitions, waveguide-fin line-waveguide, were mounted in a test fixture with transversal dimensions corresponding to the standard WR-28 waveguide and measured in the scalar bench described in section 3 of this report. The results are summarized in Table 2, showing a better performance the 1.5 λ_g taper.

FIN-LINE TO MICROSTRIP TRANSITION

Microstrip circuits have been demonstrated at frequencies up to 110 GHz [15]. In order to produce 20/30 GHz microstrip to rectangular waveguide transitions, three different configurations were initially considered, using a) waveguide post, b) tapered ridge waveguides, c) antipodal fin-lines. The last one was selected for its mechanical simplicity.

As before a double transition, waveguide-microstrip-waveguide, with central symmetry will be required for better transition characterization. The design procedure will first include X-band modeling and subsequent scaling to K_a-band.

The analysis of the rectangular waveguide-antipodal fin line-microstrip transition shown in figure 22 will be very complex, due to the existence of circuit regions where numerical methods like the spectral [16] or T.L.M. [17] will have to be applied. Three regions are well defined in the

---

[15] P. Bhartia, I. Bahl, "Millimiter Wave Engineering and Applications". J. Wiley, 1984.

[16] E. Pic, S. Tedjimi, C. Nasrallh, "Une nouvelle ligne integrable millimetrique: la ligne a ailettes". Ann Telecom Vol 37, nos 11,12, 1982, pp. 461-476.

[17] P.B. Johns, "Application of Transmission-Line Matrix Method to Homogeneous Waveguides of Arbitrary Cross-Section". Proc. Inst. Elec, Eng. Vol. 119, no 8, August 1972, pp. 1086-1091.

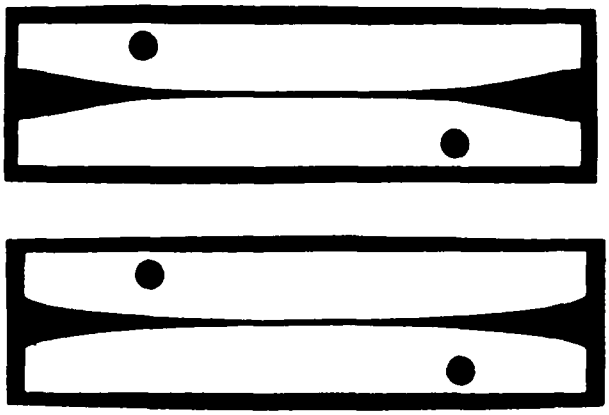

Triangular taper.

Exponential taper.

Figure 20. Ka band waveguide to fin-line 1.5 λ transition mask
(2:1 scale).

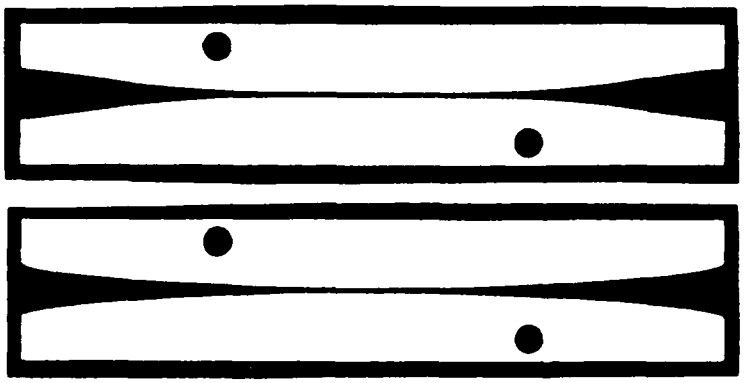

Triangular taper.

Exponential taper.

Figure 21. Ka band waveguide to fin-line 2 λ transition mask
(2:1 scale).

TABLE 2

36 GHz measurements of double transitions from rectangular waveguide to unilateral fin-line.

Transition taper	Insertion Loss (dB) (± 0.1 dB)	Return Loss (dB)
Exponential $L = 1.5\ \lambda_g$	0.8	> 28.0
Triangular $L = 1.5\ \lambda_g$	0.5	> 28.0
Exponential $L = 2\ \lambda_g$	0.9	16.3 (± 1.5 dB)
Triangular $L = 2\ \lambda_g$	0.9	16.3 (± 1.0 dB)

transition. First an antipodad tapered fin-line, with an impedance that may be approximated by the mean value of the corresponding unilateral and bilateral lines, approximation valid only for thin substrates of low dielectric constant. An intermediate region, no longer a fin-line due to the presence of the circumferential contours. Finally a microstrip, for which experimental data and analytical expressions are well known.

A series of six X-band double transitions has been produced on ten mil thick Duroid 5880 substrate and measured. A set of typical reflection and transmission measurements is shown in figure 23, indicating an acceptable performance in the range 10.2 - 12.5 GHz. Of those measured values a return loss better than 18 dB and a insertion loss better than 0.1 dB may be attributed to the tapered fin-line. The K_a-band transition mask (scale 1:1). Of figure 24 has been used in the construction of a 36 GHz transition on 0.010" Cu-Clad 217 substrate, that has the transmission an reflection losses shown in figure 25. With regard to those measurements if the microstrip losses are deducted the insertion loss curve would rise approximately 1 dB.

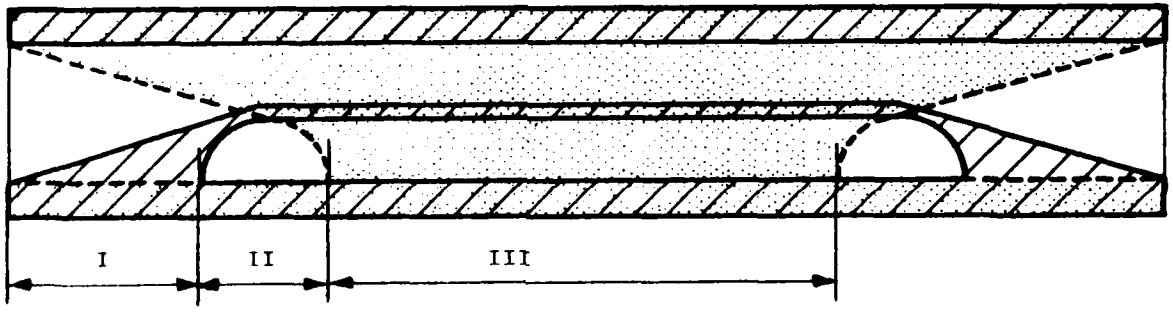

I : tapered fin-line region

II : transition region

III : microstrip region

Figure 22. Antipodal fin-line to microstrip transition.

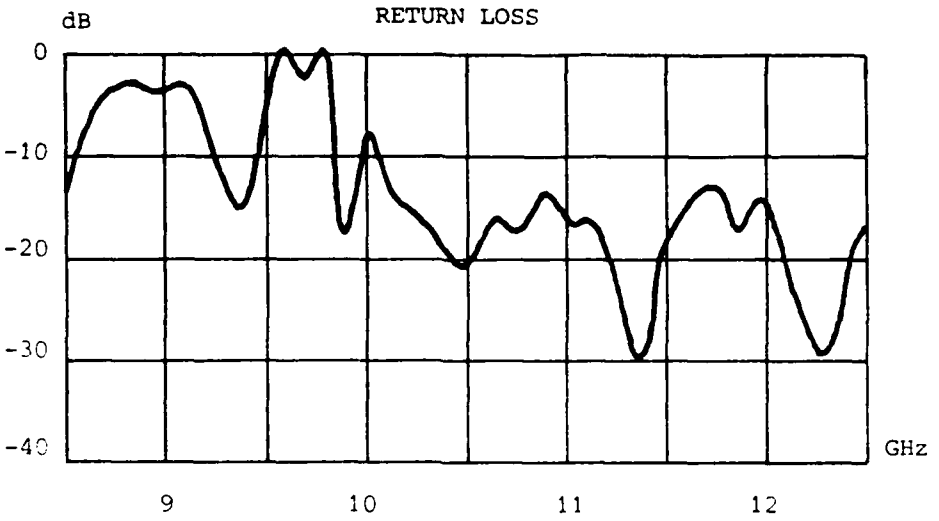

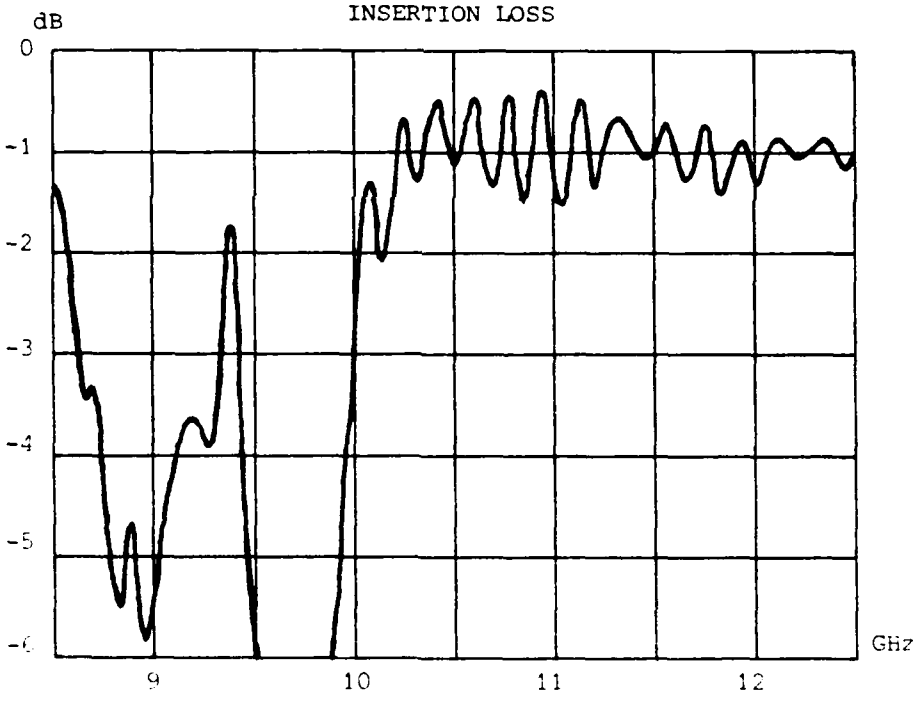

Figure 23. Fin-line to microstrip transition. Reflection and transmission measurements.

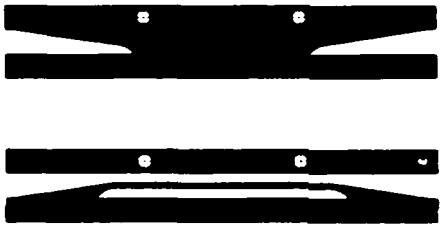

Figure 24. Ka band waveguide-finline-microstrip transition (1:1 scale).

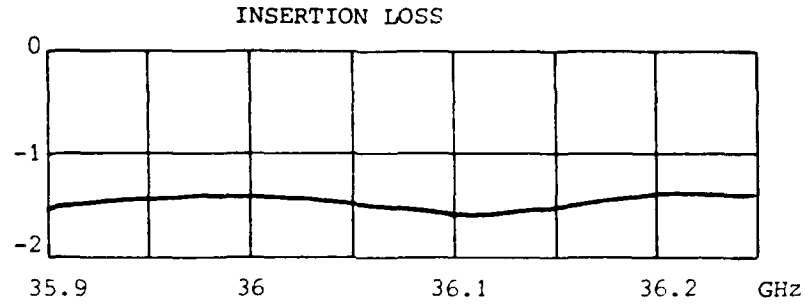

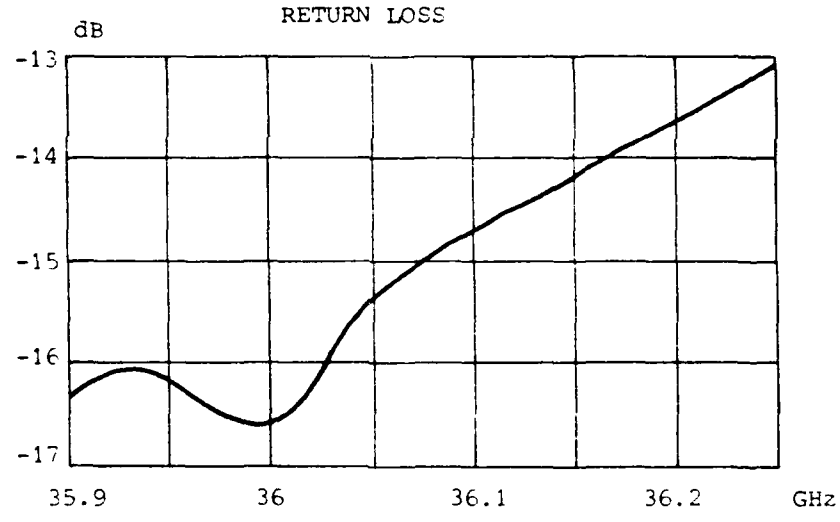

Figure 25. K_a-band fin-line to microstrip transition. Reflection and transmission measurements.

6. CYLINDRICAL NEAR - FIELD RANGE

The calculation of the radiation pattern of an antenna from near fields measurements is a technique developed over the last ten years, that brings antenna measurements fron outdoors to a laboratory setting.

The system geometry (plane, cylindrical or spherical) is conditioned, in principle, by the type of diagram under measurement, and in the last instance by the mechanical and computing resources available. Depending on the diagrama it can se stated that for pencil-beam antennas a plane system would be the most convenient, for a fan-type a cylindrical geometry will be preferred and finally a spherical surface will be well adapted to low gain antennas. Table 3 shows the advantages of the different geometries. The choice of the cylindrical one is a good compromise solution for the means available in a medium size laboratory.

A formulation for the cylindrical case has been set up, that allows the calculation of the fields over any arbitrary surface external to the antenna. An important effort has been made to make it flexible at the expense of some constraints on the measuring probe. This formulation has been used to study the influence of the different geometrical parameters that intervene in a near field measumerement [18].

ANALYTICAL EXPRESSIONS

For the cylindrical surface S_o of radius R_o, shown in figure 26, that surrounds the antenna under measure, wich can be inscribed in a minimuncylinder of radius R_a and height Z_a, an expansion of the field external to R_a in cylindrical harmonics gives

---

18 L. Jofre, A. Cardama, M. Ferrando, F. Robin, A. Heckli, Y. Michel, "A parametric Study of a Cylindrical Near-Field Antenna Measurement System" International Symposium on Antennas, Nice, 13-15 Novembre 1984

T A B L E 3

Comparison of different near-field geometries

GEOMETRY	MECHANICAL COMPLEXITY →	NUMERICAL COMPLEXITY →	APPLICATION SCOPE →
PLANE			
CYLINDRICAL			
SPHERICAL			

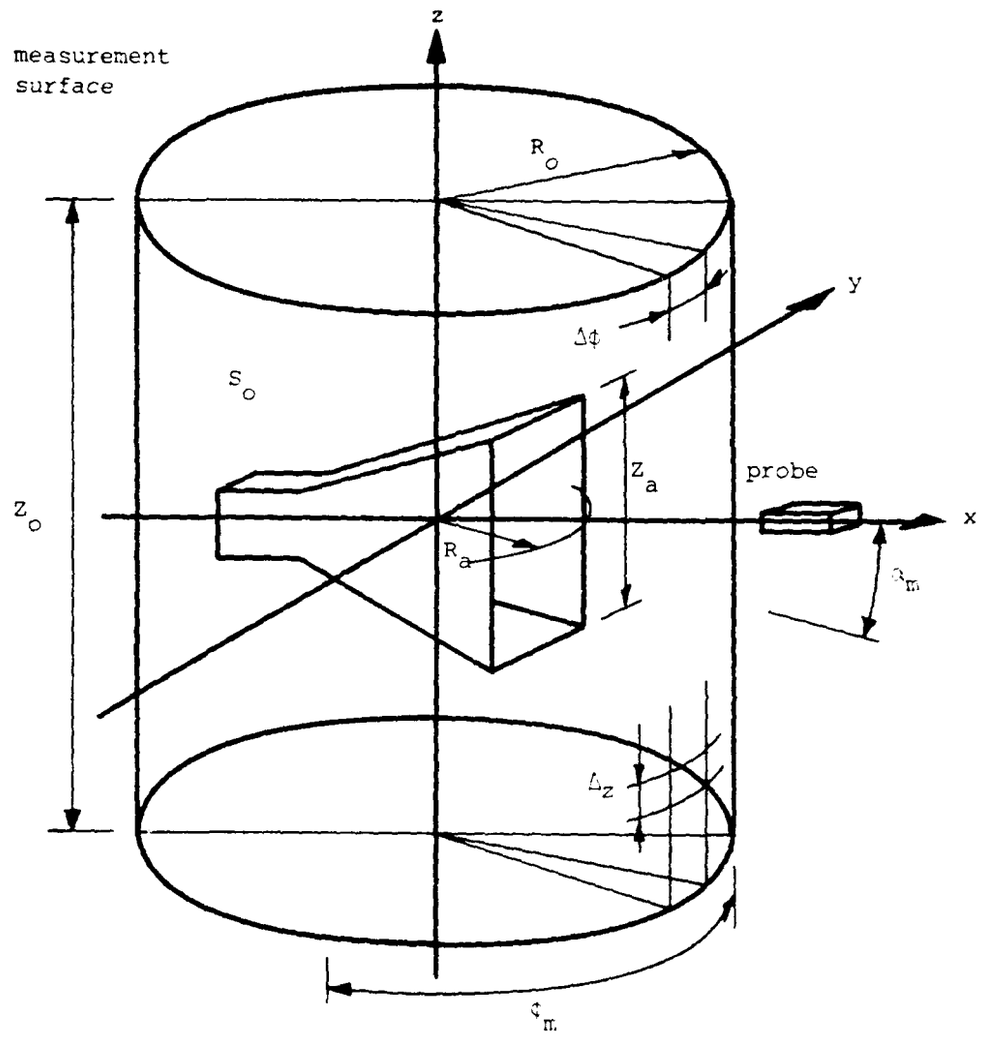

Figure 26. Cylindrical nera-field measurement geometry.

$$\vec{E}(\rho,\phi,z) = \sum_{n=-\infty}^{\infty} \int_{-\infty}^{\infty} \left[a_n(k_z)\vec{M}_n(k_z) + b_n(k_z)\vec{N}_n(k_z) \right] dk_z \quad (*)$$

with the cylindrical wave vectors $\vec{M}$, $\vec{N}$ given by

$$\vec{M}_n(k_z) = \left[\hat{\rho} \frac{jn}{\rho} H_n^{(2)}(k_\rho \rho) - \hat{\phi} \frac{\partial}{\partial \phi} H_n^{(2)}(k_\rho \rho) \right] e^{jn\phi} e^{-jk_z z}$$

$$\vec{N}_n(k_z) = \left[-\hat{\rho} \frac{jk_z}{k} \frac{\partial}{\partial \rho} H_n^{(2)}(k_\rho \rho) + \hat{\phi} \frac{nk_z}{k} H_n^{(2)}(k_\rho \rho) + \right.$$

$$\left. + \hat{z} \frac{k_\rho^2}{k} H_n^{(2)}(k_\rho \rho) \right] e^{jn\phi} e^{-jk_z z}$$

with $k = 2\pi/\lambda$, $k_z = k \cos\theta$, $k_z^2 + k_\rho^2 = k^2$

The harmonic coefficients $a_n(k_z)$, $b_n(k_z)$ may be obtained applying continuity conditions over the surface of measurement S_o. For the magnetic fields, if an electrically small probe is used, such that the antenna is placed in its far-field and the diagram approximates in boresight that of an elementary magnetic dipole, it results in

$$a_n(k_z) = \frac{\pi k \, j^{-(n+1/2)}}{k_\rho^2 F(\psi_n)} \bar{H}_z(n, k_z)$$

$$b_n(k_z) = \frac{\pi \, j^{-(n-1/2)}}{k_\rho F(\psi_n) \cos\psi_n} \left[\bar{H}_\phi(n,k_z) + \frac{k_z \sin\psi_n}{k_\rho} \bar{H}_z(n, k_z) \right]$$

with

$$\psi_n = - \sin^{-1} \left(\frac{n}{k_\rho R_o} \right)$$

$$F(\psi_n) = \sqrt{\frac{2\pi}{k_\rho R_o \cos\psi_n}} \; e^{-j(k_\rho R_o \cos\psi_n - n\psi_n)}$$

$$\bar{H}_{\phi,z}(n,k_z) = \int_{-\pi}^{\pi} e^{-jn\phi} \, d\phi \int_{-\infty}^{\infty} H_{\phi,z}(R_o,\phi,z) \, e^{jk_z z} \, dz$$

$H_{\phi,z}$ being the ϕ and z components of the magnetic field measured over S_o. (Similar expressions may be derived for the electric field).

From (*) the field in any point external to the antenna may be reconstructed, in particular over its surface. For the far fields (*) simplifies to

$$E_\theta(\theta,\phi) = - 2k \sin\theta \frac{e^{-jkr}}{r} \sum_{|n|<k R_o \sin\theta} j^{n+1} e^{jn\phi} b_n(k \cos\theta)$$

$$E_\phi(\theta,\phi) = - j \, 2k \sin\theta \frac{e^{-jkr}}{r} \sum_{|n|<k R_o \sin\theta} j^{n+1} e^{jn\phi} a_n(k \cos\theta)$$

X-BAND PARAMETRIC STUDY

To show the validity of this formulation, and evalatue the effect of the different parameters on near-field measurements, an experimental study in X-band (8-12 GHz) was performed [18], with the main results compiled in Table 4.

T A B L E 4

X-Band cylindrical near-field range parameters

Geometrical	Electrical	Mechanical
$Z_o = Z_a + 2\ (R_o - R_a) tg\ \alpha_m$	frequency stability: $\pm\ 10^{-5}$	lineal accuracy: $\pm\ \lambda/50$
$\Delta z = \frac{\lambda/2}{\sin \alpha_m}$	amplitud accuracy: $\pm$ 0.05/10 dB	angular accuracy: $\pm$ 0.06 deg
$\phi_o > \phi_m$		
$\Delta\phi = \frac{\lambda}{2\ R_a}$	phase accuracy: $\pm$ 0.4deg/10 dB	
$R_o - R_a > 10\ \lambda$	probe: WR-28 waveguide loaded with $\varepsilon' = 9$	

Those results have been established for a diagram accuracy of ± 1 dB down to the -30 dB level. The geometrical parameters refer to figure 26, with α_m, ϕ_m defining in elevation and azimuth the angular region where the diagram of the antenna is to be obtained accurately.

As a probe an open-ended dielectric loaded waveguide was used, figure 27, presenting in its frontal region a diagram that approximates precisely that of an elementary magnetic dipole.

SPECIFICATION OF THE 20/30 GHz SYSTEM

The preceeding X-Band results have been scaled to 20/30 GHz and used to define the characteristics of a cylindrical system for the measurement of parabolic antennas with diameters up to 120 cm. In table 5 a comparison is made at both frequencies between the values needed and those expected in our installation.

Figure 28 shows the system's configuration, including linear and angular positioners, driven by step motors, fitted with an intelligent controler (Superior Electric). The mobile probe is connected to the receiver with a flexible coaxial cable of high stability in both phase and amplitude (GORE-TEX RGH), dispensing with the use of rotary joints. Althougt the system will work up to 30 GHz, the sweeper-receiver installed at this time (HP 83590 A - HP 8410 C) limits its maximum operating frequency to 20 GHz.

Further work will be required in the following areas:

a) Desing, construction and test of open-ended dielectric-loaded probes.

b) Automatization of the system with a µC HP-85.

c) The study of alternative measurement methods using multiplexing techniques, in particular the modulated scattering technique, that may produce an important reduction in time.

T A B L E 5

20/30 GHz Cylindrical near-field range parameters

	20 GHz	30 GHz	Target
lineal accuracy	± 0.3 mm	± 0.2 mm	± 0.1 mm
angular accuracy	± 0.03°	± 0.02°	± 0.02°
length (Z_o)	-	-	1400 mm
probe (waveguide)	WR - 15 $\varepsilon' = 9$	WR - 10 $\varepsilon' = 9$	-

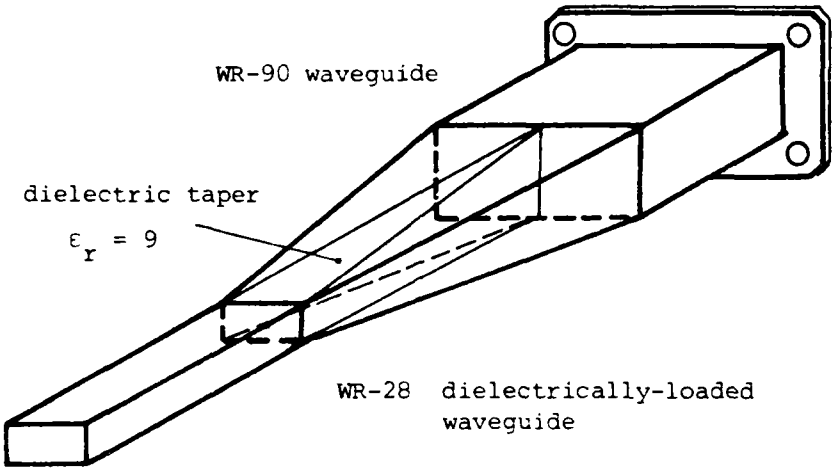

Figure 27. Near-field probe.

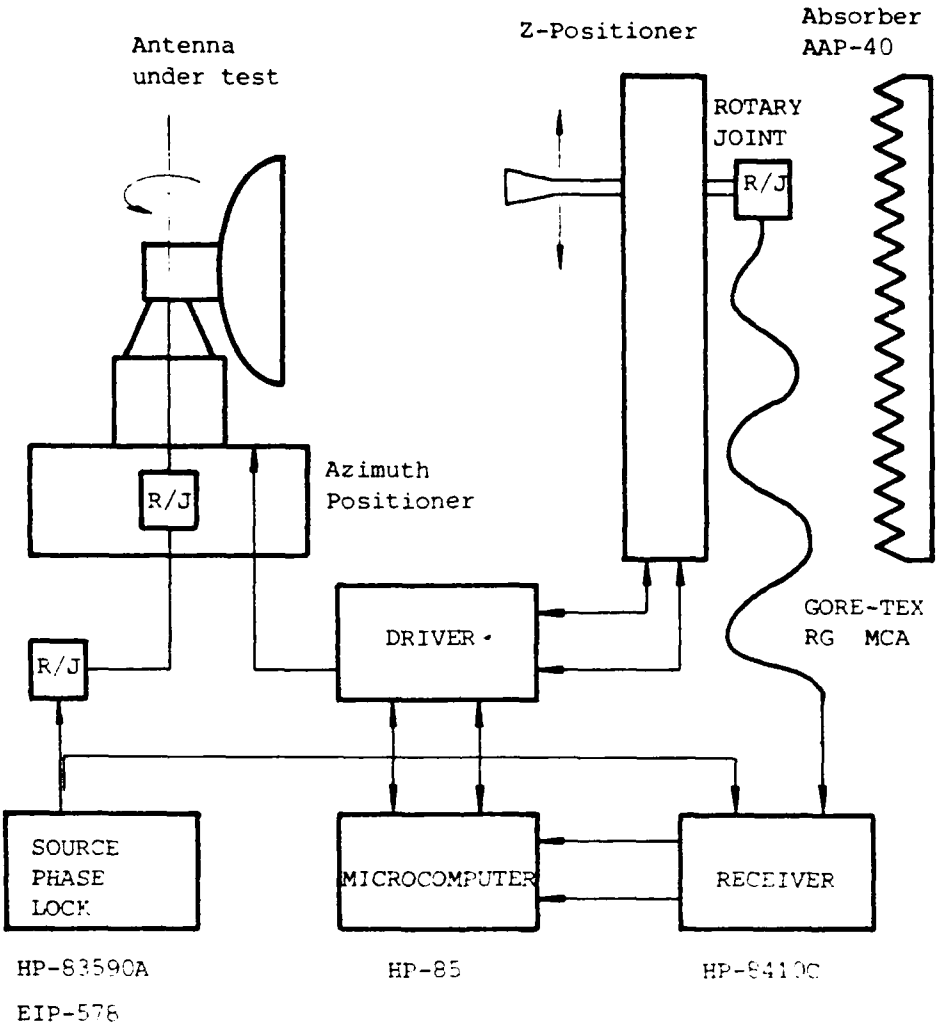

Figure 28. Cylindrical near-field measurement system

7. CONCLUSIONS AND RECOMMENDATIONS

In conclusion the first year of the system's development program has permitted the acquisition of the basic skills required for the design and measurement of 20/30 GHz microwave circuits and antennas.

Concerning the receiver design, the analysis of the possible configurations has led to consider two distinct options. The complexity of the technical and economical implications of the selection of one of them, disclosed by this analysis, deserves further study. This work will be completed in the next few months, proceeding then to set the final specifications and the selection of the receiver configuration.

The operative measurement systems, automatic network analyzer useful up to 20 GHz, manual scalar reflection and transmission benches at 36 GHz and vector reflection system at the same frequency, will be completed with a full k_a-band vector reflection and transmission system in process of implementation.

Two different waveguide-mounted Gunn diode oscillators in the k_a band have been constructed and tested. The possibility of developing Gunn-oscillators with diodes mounted on microstrip lines and subharmonically injection locked to high stability sources is being considered. In this regard modelling at X-band has started with the non-linear characterization of the diode.

Fin-line structures have been analyzed and an approximation for the effective dielectric constant has been proposed in the range of linewidths where closed expressions have not been found. A number of fin-line tapers have been studied and constructed, showing a performance in acordance with expected values. Those structures will be used, among other applications, on pin modulators.

The antenna measurement systems study has produced protocol and software developments for a cylindrical near field system and electrical and mechanical specifications for a 20/30 GHz range. Near-field probe design using dielectric-loaded waveguides has also been completed.

In order to complete the system before the satellite is operational the following tasks should be undertaken during the second year: setting the final specifications and configuration of the receiver, making operational the cylindrical near-field system, and continued antenna development and work on passive and active circuits.

END

FILMED

1-85

DTIC